

# Combined Experimental and Computational Study on the Unimolecular Decomposition of JP-8 Jet Fuel Surrogates. I. *n*-Decane (*n*-C<sub>10</sub>H<sub>22</sub>)

Long Zhao, Tao Yang<sup>1</sup> and Ralf I. Kaiser<sup>2\*</sup>

Department of Chemistry, University of Hawaii at Manoa, Honolulu, Hawaii 96822, United States

Tyler P. Troy and Musahid Ahmed<sup>2\*</sup>

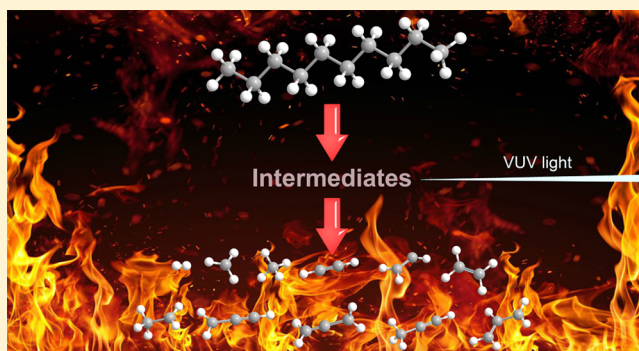
Chemical Sciences Division, Lawrence Berkeley National Laboratory, Berkeley, California 94720, United States

Daniel Belisario-Lara, Joao Marcelo Ribeiro, and Alexander M. Mebel<sup>2\*</sup>

Department of Chemistry and Biochemistry, Florida International University, Miami, Florida 33199, United States

## Supporting Information

**ABSTRACT:** Exploiting a high temperature chemical reactor, we explored the pyrolysis of helium-seeded *n*-decane as a surrogate of the *n*-alkane fraction of Jet Propellant-8 (JP-8) over a temperature range of 1100–1600 K at a pressure of 600 Torr. The nascent products were identified *in situ* in a supersonic molecular beam via single photon vacuum ultraviolet (VUV) photoionization coupled with a mass spectroscopic analysis of the ions in a reflectron time-of-flight mass spectrometer (ReTOF). Our studies probe, for the first time, the *initial* reaction products formed in the decomposition of *n*-decane—including reaction radicals and thermally labile closed-shell species effectively excluding mass growth processes. The present study identified 18 products: molecular hydrogen (H<sub>2</sub>), C<sub>2</sub> to C<sub>7</sub> 1-alkenes [ethylene (C<sub>2</sub>H<sub>4</sub>) to 1-heptene (C<sub>7</sub>H<sub>14</sub>)], C<sub>1</sub>–C<sub>3</sub> radicals [methyl (CH<sub>3</sub>), vinyl (C<sub>2</sub>H<sub>3</sub>), ethyl (C<sub>2</sub>H<sub>5</sub>), propargyl (C<sub>3</sub>H<sub>3</sub>), allyl (C<sub>3</sub>H<sub>5</sub>)], small C<sub>1</sub>–C<sub>3</sub> hydrocarbons [methane (CH<sub>4</sub>), acetylene (C<sub>2</sub>H<sub>2</sub>), allene (C<sub>3</sub>H<sub>4</sub>), methylacetylene (C<sub>3</sub>H<sub>4</sub>)], along with higher-order reaction products [1,3-butadiene (C<sub>4</sub>H<sub>6</sub>), 2-butene (C<sub>4</sub>H<sub>8</sub>)]. On the basis of electronic structure calculations, *n*-decane decomposes initially by C–C bond cleavage (excluding the terminal C–C bonds) producing a mixture of alkyl radicals from ethyl to octyl. These alkyl radicals are unstable under the experimental conditions and rapidly dissociate by C–C bond β-scission to split ethylene (C<sub>2</sub>H<sub>4</sub>) plus a 1-alkyl radical with the number of carbon atoms reduced by two and 1,4-, 1,5-, 1,6-, or 1,7-H shifts followed by C–C β-scission producing alkenes from propene to 1-octene in combination with smaller 1-alkyl radicals. The higher alkenes become increasingly unstable with rising temperature. When the C–C β-scission continues all the way to the propyl radical (C<sub>3</sub>H<sub>7</sub>), it dissociates producing methyl (CH<sub>3</sub>) plus ethylene (C<sub>2</sub>H<sub>4</sub>). Also, at higher temperatures, hydrogen atoms can abstract hydrogen from C<sub>10</sub>H<sub>22</sub> to yield *n*-decyl radicals, while methyl (CH<sub>3</sub>) can also abstract hydrogen or recombine with hydrogen to form methane. These *n*-decyl radicals can decompose via C–C bond β-scission to C<sub>3</sub> to C<sub>9</sub> alkenes.



## 1. INTRODUCTION

Kerosene-based jet fuel JP-8 presents the single battlefield fuel for the US Air Force and Army equipment. It consists of several hundred hydrocarbons, which can be grouped into four main classes: (i) aliphatic “paraffins” (33–61% *n*-alkanes and isoalkanes; 1–5% olefins), (ii) monocyclic “paraffins” (10–20%), (iii) alkyl-substituted benzenes (12–22%), and (iv) polycyclic aromatic hydrocarbons (PAHs) (10–20%); additives acting as fuel system icing inhibitors, corrosion inhibitors, and static dissipaters at the subpercent level complement the

mixture.<sup>1–11</sup> Because of the chemical complexity of JP-8, engineering and combustion scientists have been searching for surrogate fuels that can reasonably represent the performance and emissions behavior of JP-8 jet fuel engines thus providing a baseline for performance and emissions.<sup>12–23</sup> The scientific community concluded that accurate modeling of the

Received: November 15, 2016

Revised: January 6, 2017

Published: January 16, 2017

combustion of JP-8 jet fuel is currently not feasible due to the chemical complexity. Therefore, surrogate fuel and their mixtures are considered as a key step toward modeling and understanding the combustion of practical aviation fuel (Figure 1).<sup>3,24–26</sup> Single-component fuels are adequate for simple

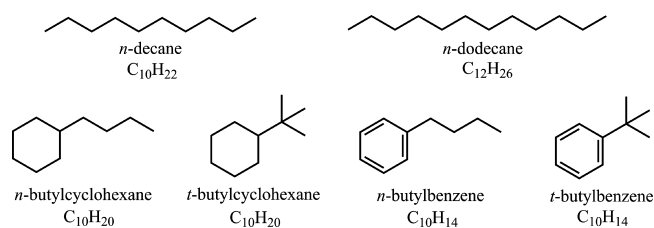


**Figure 1.** Molecular structures of prototype surrogates covering three main classes of molecules present in JP-8 based fuel: alkanes (*n*-decane ( $C_{10}H_{22}$ ), *n*-dodecane ( $C_{12}H_{26}$ )), cycloalkanes (*n*-butylcyclohexane ( $C_{10}H_{20}$ ), *tert*-butylcyclohexane ( $C_{10}H_{20}$ )), and alkyl-substituted benzenes (*n*-butylbenzene ( $C_{10}H_{14}$ ), and *tert*-butylbenzene ( $C_{10}H_{14}$ )).

applications like combustion efficiency, while multicomponent surrogates are required for chemistry-dependent applications such as soot formation and emissions, combustion staging, and numerical modeling of flames.<sup>27</sup>

The development of these chemical kinetic models requires accurate input parameters and an intimate understanding of the very first processes, which initiate bond rupture processes in JP-8 surrogates, provide a pool of radicals, and control the autoignition, under realistic, combustion relevant physical conditions.<sup>10,26,28–30</sup> These are typically temperatures up to 1600 K and pressures up to a few atmospheres. In principle, the unimolecular decomposition and “pyrolysis” of these surrogates leads to smaller hydrocarbon molecules and reactive transient species, among them aliphatic radicals, resonantly stabilized free radicals (RSFRs), and aromatic radicals (ARs), which initiate and drive the complex chemistry in the combustion of JP-8 based jet fuel. Here, the initial decomposition chemistry is often dubbed as “delivering the building blocks” for the oxidation of JP-8 based jet fuel. Nevertheless, despite decades of research, the fundamental question “What are the basic, most fundamental processes, which initiate the combustion of JP-8 based jet fuel?” has not been resolved to date, predominantly because well-defined experimentally derived mechanistic information and identification of the nascent pyrolysis products are lacking with about 95% of the reaction pathways in models being “assumed”; this even holds for sophisticated chemical kinetic models of *n*-alkane surrogates such as *n*-decane and *n*-dodecane.<sup>31–37</sup> However, detailed data on the mechanism and products formed in the initial decomposition steps of JP-8 based fuel components are crucial to elucidate the underlying reaction mechanisms how JP-8 based engines are operating. Therefore, an innovative approach is carried out here to investigate the decomposition (“pyrolysis”) of prototype JP-8

jet fuel surrogates and to probe the nascent product(s) together with the underlying mechanisms comprehensively thus advancing the current understanding of these fundamental, elementary processes, which initiate and drive the complex chemistry in the combustion of JP-8 based jet fuel.

We describe the complex processes that JP-8 surrogates undergo upon pyrolysis with a survey of previous results. Malewicki and Brezinsky<sup>38</sup> conducted high pressure (14 440 to 56 240 Torr) *n*-decane and *n*-dodecane pyrolysis and oxidation experiments in shock tubes (Tables 1 and S1 in the Supporting Information). Qi et al.<sup>39</sup> presented a comprehensive study on *n*-decane pyrolysis and oxidation at 5, 30, 150, and 760 Torr along with premixed laminar flames at equivalence ratios of 0.7, 1.0, and 1.8. In both experiments, tunable vacuum ultraviolet photoionization mass spectrometry (VUV-PIMS)<sup>40–48</sup> was exploited to identify and to quantify the species formed. Zeppieri et al.<sup>49</sup> set up a series of *n*-decane oxidation and pyrolysis experiments in the Princeton Atmospheric pressure flow reactor. For pyrolysis studies, the authors exploited 1060 K at a pressure of 760 Torr and inlet mole fraction of *n*-decane to be 1456 ppm. Zhou et al.<sup>50</sup> presented an experimental and modeling investigation of *n*-decane pyrolysis at supercritical pressures at the temperature range from 773 to 943 K and pressures of 22 500, 30 000, and 37 500 Torr. This study exposed that *n*-decane was mainly consumed via hydrogen abstraction reactions followed by  $\beta$ -scission to form smaller C1 to C6 products. They also conducted pressure-dependent flow reactor experiments of the pyrolysis of *n*-decane exploiting VUV-PIMS to identify the species and their mole fractions.<sup>51</sup> Finally, Jiang et al.<sup>52</sup> investigated the thermal decomposition of *n*-decane at supercritical pressures in a flow reactor detecting multiple hydrocarbons from C1 to C10. In summary, previous studies were conducted at temperatures from 773 to 1731 K, pressures covering 35 to 39 603 Torr, and residence times up to 7600 ms (Tables 1 and S1). Note that mechanistic studies were also carried out by shifting the focus from “macroscopic” setups (shock tubes, jet-stirred reactors, flames) to the “microscopic” level (molecules). Two studies probed the decomposition rates of *n*-decane between 918 and 958 K<sup>53</sup> and from 713 to 793 K.<sup>54</sup> However, the activation energies of the C–C bond rupture processes differed greatly from 260 to 111 kJ mol<sup>−1</sup>; products were not sampled in these experiments.

Besides the experimental studies as compiled in Tables 1 and S1, high-level theoretical data on the structure and energetics of the surrogate molecules and their decomposition products are sparse owing to their relatively large molecular size. Multiple combined experimental and theoretical studies devoted to the conformational stability and the molecular shape, rotational constants, and ionization energies of *n*-decane and *n*-dodecane were conducted.<sup>55</sup> Considering the thermochemical properties, density functional theory (DFT) calculations were performed to evaluate the enthalpy of formation of *n*-decane and *n*-

**Table 1.** Compilation of Previous Experimental Studies on the Pyrolysis of *n*-Decane

group	method	temperature (K)	pressure (Torr)	residence time (ms)	ref
Brezinsky et al.	shock tube	947–1731	35 492–56 392	1.27–1.90	38
Qi et al.	flow reactor	786–1505	5, 30, 150 and 760	2.17–211	39
Zeppieri et al.	flow reactor	1060	760	0–300	49
Zhou et al.	supercritical flow reactor pyrolysis	773–943	22 502–37 503	150–600	50
Zhou et al.	flow reactor	786–1378	30, 150, and 760	3.8–164	51
Jiang et al.	flow reactor	862–903	31 502–39 603	–	52

dodecane together with their C–C bond dissociation energies.<sup>56</sup> The MPW1B95/6-311G(d,p) method was found to compute the enthalpies of formation along with the C–C bond dissociation energies satisfactorily. Also, Hirao and co-workers revealed via calculations of isodesmic reaction energies of alkanes including those of *n*-decane that the use of conventional DFT reveals errors of up to 3 kJ mol<sup>-1</sup> for *n*-decane.<sup>57</sup> These errors originate mainly from the limited description of intramolecular van-der-Waals interactions and might be overcome by exploiting long-range corrected DFT methods or even coupled cluster based approaches.

Finally, we would like to address briefly modeling studies on the JP-8 surrogate *n*-decane. Ranzi et al.<sup>58</sup> generated a wide-range kinetic modeling study of the pyrolysis, partial oxidation, and combustion of *n*-alkanes including *n*-decane, *n*-dodecane, and *n*-hexadecane. The model was developed from the complete set of primary propagation reactions via the MAMOX++ program code, which is used for automatically generating all of the primary decomposition and oxidation steps of normal and branched paraffins.<sup>59</sup> The proposed lumping technique simplified the description of the primary products and resulted in an easier description of the successive reactions of the intermediates. Westbrook et al.<sup>60</sup> developed detailed kinetic mechanisms for the pyrolysis and oxidation of *n*-alkanes up to *n*-hexadecane (C<sub>16</sub>H<sub>34</sub>) with both low- and high-temperature reactions considered. These authors tested the mechanisms against several experimental data including oxidation in a jet-stirred reactor, shock tube ignition, and flow reactor oxidation.<sup>38,39,50,51,61</sup> Dooley et al.<sup>61</sup> set up a detailed kinetic model incorporating mechanisms for toluene, *n*-alkane, isoalkane, and C1–C4 species, in which the mechanisms of the *n*-alkane was taken from Westbrook et al.<sup>60</sup> The model by Dooley et al. was revised by Malewicki et al.<sup>38</sup> to predict the high pressure shock tube pyrolysis and oxidation of *n*-decane. Qi et al.<sup>39</sup> also set up a new detailed kinetic model of *n*-decane pyrolysis and combustion with 234 species and 1452 reactions and validated the model with several literature experimental data including flow reactor, shock tube reactor, premixed laminar flame, counterflow diffusion flame, laminar flame speed, and ignition delay times. This work was a comprehensive experimental and modeling investigation on *n*-decane, unravelling its pyrolysis and oxidation properties at both low and high pressures. Finally, Jia et al.<sup>51</sup> assembled the sub mechanisms of *n*-decane<sup>39</sup> and nitromethane to simulate the flow reactor for *n*-decane pyrolysis initiated by nitromethane.

However, the summary of the previous studies suggests that an understanding of the unimolecular decomposition of single component JP-8 fuel surrogates (Figure 1 and Tables 1 and S1)—even as simple as *n*-decane—is incomplete both from the experimental and theoretical viewpoints. Whereas these investigations yielded valuable information on the formation of closed-shell hydrocarbon intermediates and products, these species were mainly analyzed off-line and *ex situ* (HPLC, GC MS); neither HPLC nor GCMS can sample radical transient species nor thermally labile closed-shell molecules. Therefore, the “molecular inventory” might have been altered since its formation, crucial reaction intermediates cannot be sampled, and detailed information on the reaction mechanisms—the role of radicals and intermediates—cannot always be obtained, but are at best inferred indirectly and qualitatively. Likewise, a simultaneous *online* and *in situ* probing of *all* transient species and closed-shell products via laser techniques or spectroscopy is

currently beyond the scope of any simulation experiment; recall that spectroscopic detection schemes like laser-induced fluorescence (LIF) and Rydberg tagging (H, D, O) are restricted to species with well-established spectroscopic fingerprints, which are typically smaller, di- and triatomic species. It is therefore not surprising that the present kinetic models of the pyrolysis of surrogate fuels, such as for example those for *n*-alkanes<sup>60</sup> are mostly based on the thermochemical data and activation energies estimated from group additivity schemes or from molecular dynamics simulations with empirical reactive force fields like ReaxFF.<sup>62</sup> On the basis of these considerations, a novel methodology to investigate the unimolecular decomposition of JP-8 fuel surrogates is necessary. This approach requires probing the open- and closed-shell products *online* and *in situ* without changing the initial “molecular inventory” and exploiting versatile, nonspectroscopic detection systems so that the complete product spectrum can be sampled quantitatively. These studies will be combined with electronic structure calculations to yield a unified picture on the temperature and pressure dependent decomposition mechanisms of JP-8 jet fuel surrogates.

The present investigation represents the first in a series of combined experimental and theoretical studies to probe the pyrolysis and decomposition of prototype JP-8 jet fuel surrogates: *n*-decane (C<sub>10</sub>H<sub>22</sub>). Here, the pyrolysis is explored in a high temperature chemical reactor, in which the decomposition of jet fuel surrogates can be probed systematically under combustion-like temperatures up to 1600 K.<sup>63</sup> The nascent product distribution - including radicals and thermally labile closed-shell species - are probed *online* and *in situ* in a supersonic molecular beam exploiting soft photoionization with single photon VUV light followed by a mass spectroscopic analysis of the ions in a ReTOF.<sup>63–72</sup> By limiting the residence time in the reactor to a few microseconds, we aim to probe the *initial reaction products* and attempt to exclude successive (higher order) reactions of the initially formed species, which may lead to molecular mass growth processes. Finally, by carrying out molecular beam experiments and combining these studies with electronic structure calculations, we elucidate data on the products, their branching ratios, and reaction mechanisms involved in the decomposition of JP-8 surrogates over a broad range of combustion-relevant temperatures and pressures.

## 2. EXPERIMENTAL APPROACH

The experiments were conducted at the Advanced Light Source (ALS) at the Chemical Dynamics Beamline (9.0.2.) exploiting a “pyrolytic reactor”.<sup>63–73</sup> Briefly, the high temperature chemical reactor consists of a resistively heated silicon carbide (SiC) tube of 20 mm in length and 1 mm inner diameter. A gas mixture at a pressure of 600 Torr containing 0.022% decane (C<sub>10</sub>H<sub>22</sub>) (Aldrich; 99%+) in helium carrier gas (He; Airgas; 99.999%) is prepared by bubbling helium gas through *n*-decane stored in a stainless-steel bubbler held at 268 ± 1 K; at this temperature, *n*-decane has a vapor pressure of 0.132 Torr. The gas mixture was introduced into a SiC tube held at distinct temperatures from 1100 K to 1600 ± 5 K in steps of 100 K, as monitored by a Type-C thermocouple. After exiting the pyrolytic reactor, the molecular beam, containing the pyrolysis products, passes a 2 mm skimmer and enters a detection chamber containing a Wiley–McLaren ReTOF mass spectrometer. The products were then photoionized in the extraction region of the spectrometer by exploiting quasi-continuous tunable vacuum

ultraviolet (VUV) synchrotron light and detected with a microchannel plate (MCP). Here, mass spectra were taken in 0.05 eV intervals from 8.00 to 11.50 eV. A set of additional mass spectra was also measured at 15.5 eV to determine hydrogen and methane yields, which cannot be ionized at 11.5 eV. The photoionization efficiency (PIE) curves, which report the intensity of a single mass-to-charge ratio ( $m/z$ ) versus the photon energy, were extracted by integrating the signal collected at a specific  $m/z$  selected for the species of interest over the range of photon energies in 0.05 eV increments and normalized to the incident photon flux. The supersonically cooled nature of the beam of the product molecules presents a crucial prerequisite for their detection since they are rotationally and vibrationally cooled in the expansion. The residence time of *n*-decane in the reactor tube (20 mm) under our experimental condition are tens of  $\mu$ s. Pressures in the reactor were suggested at axial distances of 10 mm and 15 mm from the inlet to drop to about 60% and 30% of the inlet pressure.<sup>74</sup> This would result in typically three to four (1600 K) collisions of a decane molecule with the helium atoms at these distances. In Qi's work,<sup>39</sup> the authors presented a comprehensive studies on *n*-decane pyrolysis and *n*-decane oxidation both experimentally and theoretically. With longer residence times and enhanced initial concentrations of *n*-decane, bimolecular reactions play a significant (unwanted) role in the fuel consumption.

PIE curves are the most important features for the synchrotron vacuum ultraviolet photoionization mass spectrometer diagnosis method in combustion studies.<sup>41,46,48,75–77</sup> The PIE curves are exploited to unambiguously identify decomposition intermediates including radicals and closed-shell products. In this work, the PIE curves were extracted in the energy range from 8.0 to 11.5 eV, which covers the ionization energies (IE) of most species generated in the pyrolysis process except molecular hydrogen (IE = 15.40 eV) and methane (IE = 12.61 eV). If only one species contributes to the signal at a selected  $m/z$ , this species can be identified just based on the comparison between the experimentally recorded PIE and literature data. However, if several species contribute to the PIE, it has to be fit by a linear combination of multiple isomers which can contribute to the specific  $m/z$ . In this work, the PIE curves are taken from ref 78. For each temperature, the PIE scans were recorded three times and averaged; the experimental uncertainties were derived within one sigma as shown in the shaded areas in Figures 3–9.

In order to calculate the branching ratios of the products, the following relationship between the integrated ion intensity of species  $i$  ( $S_i(T, E)$ ) normalized by photon flux, the mole fraction ( $X_i(T)$ ), the photoionization cross section of species  $i$  at a selected photon energy ( $\sigma_i(E)$ ), and the mass discrimination factor ( $D_i$ ) has to be accounted for:

$$S_i(T, E) \propto X_i(T) \sigma_i(E) D_i \quad (1)$$

At a well-defined temperature, eq 1 can be transformed to eqs 2 and 3 essentially expressing the relationship between the mole fraction of species  $i$  and  $j$ ,

$$\frac{S_i(T, E)}{S_j(T, E)} = \frac{X_i(T) \sigma_i(E) D_i}{X_j(T) \sigma_j(E) D_j} \quad (2)$$

$$\frac{X_i(T)}{X_j(T)} = \frac{S_i(T, E) \sigma_j(E) D_j}{S_j(T, E) \sigma_i(E) D_i} \quad (3)$$

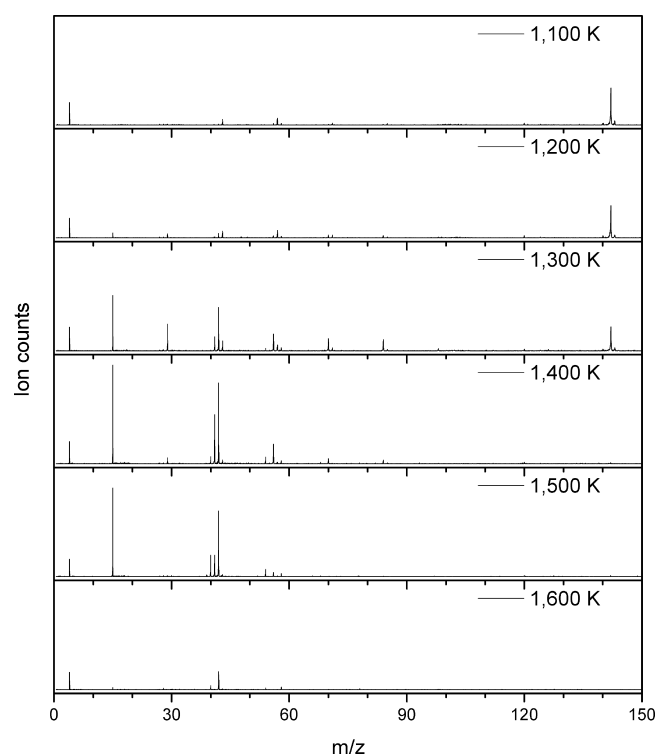


**Figure 2.** Mass spectra of the products obtained from the decomposition of *n*-decane recorded at a photon energy of 10.0 eV at different temperatures from 1100 to 1600 K.

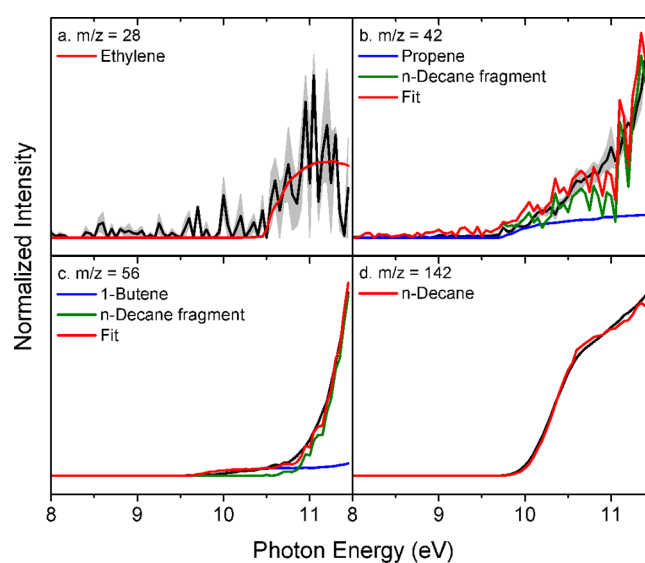


**Figure 3.** Experimental photoionization efficiency (PIE) curves (black lines) recorded from the decomposition of *n*-decane at 1100 K along with the experimental errors (gray area) and the reference PIE curves (red, green and blue lines). In the case of multiple contributions to one PIE curve, the red line represents the sum of all the contributions to the overall fit.

The branching ratios  $R_i$  of the products can be then computed via eq 4:

$$R_i = \frac{X_i}{\sum X_i} \quad (4)$$

In this work, the branching ratios were determined for selected photoionization energies of 9.0, 9.5, 10.0, 10.5, 11.0, 11.5, and

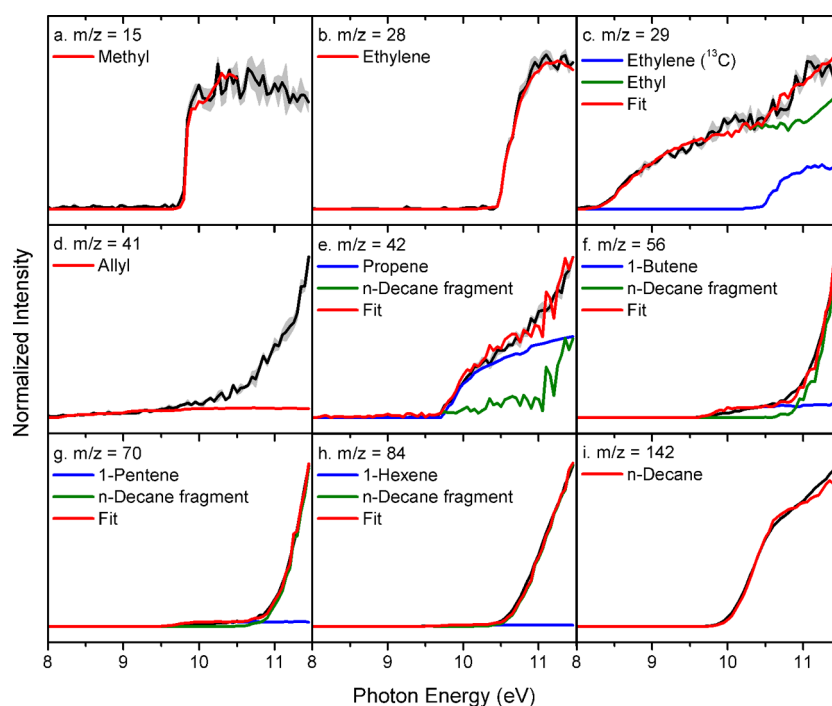


**Figure 4.** Experimental photoionization efficiency (PIE) curves (black lines) recorded from the decomposition of *n*-decane at 1200 K along with the experimental errors (gray area), and the reference PIE curves (red, green and blue lines). In the case of multiple contributions to one PIE curve, the red line indicates the sum of contributions. For  $m/z = 41$ , there may be photoionization fragments from products causing the experimental values to be higher than the fitting at higher photon energies.

15.5 eV with data obtained at 15.5 eV used to calculate the branching ratios of methane and hydrogen. The mass discrimination factors were taken from ref 73. The uncertainties of the photoionization cross sections of 15–20% were also taken into consideration.<sup>75</sup> In this work, the uncertainties of the cross section are chosen as 20%. For the allyl radical ( $C_3H_5$ ), the literature PIE curve was found to be limited in photon energy range. Therefore, a new PIE scan for the allyl radical was recorded to collect a PIE curve from 7.5 to 11.5 eV. For this, allyl iodide ( $C_3H_5I$ , Sigma-Aldrich, 98%) was seeded in 600 Torr of helium carrier gas at a fraction of 0.0025% allyl iodide. The PIE curve was extracted for  $m/z = 41$ . The temperature of the SiC tube was kept at 827 K to cleave the C–I bond of allyl iodide to generate the allyl radical.

### 3. COMPUTATIONAL METHODS

Geometries of *n*-decane and its primary and secondary decomposition products as well as transition states for secondary decomposition reactions (isomerizations and C–C and C–H bond  $\beta$ -scissions) and for direct hydrogen atom abstractions by hydrogen atoms have been optimized using the density functional B3LYP method with the 6-311G(d,p) basis set. Vibrational frequencies of various local minima and transition states have been computed at the same level of theory. Relative energies for all species have been refined by single-point calculations at the G3(CCSD,MP2) level of theory,<sup>79–81</sup> which included the empirical higher level correction (HLC),<sup>81</sup> using B3LYP/6-311G(d,p) optimized geometries and including zero-point vibrational energy corrections (ZPE) also obtained at B3LYP/6-311G(d,p). The inclusion of the HLC increases the calculated strengths of C–H bonds by 7 kJ mol<sup>-1</sup>, decreases relative energies of transition states and products for the  $C_{10}H_{22} + H \rightarrow C_{10}H_{21} + H_2$  hydrogen atom abstraction reactions also by 7 kJ mol<sup>-1</sup>, is

insignificant for C–C bond cleavages, and zero by definition for C–C bond  $\beta$ -scissions. The G3(CCSD,MP2)//B3LYP theoretical level is expected to provide the energetic parameters with “chemical accuracy” within 3–6 kJ mol<sup>-1</sup> in terms of average absolute deviations.<sup>81</sup> The ab initio calculations were performed using the GAUSSIAN 09<sup>82</sup> and MOLPRO 2010<sup>83</sup> program packages.

Rate constants for various primary and secondary reactions involved in the pyrolysis of *n*-decane have been computed by solving the one-dimensional master equation<sup>84</sup> employing the MESS package.<sup>85</sup> Here, rate constants  $k(T)$  for individual reaction steps were calculated within RRKM (unimolecular reactions) or transition state theory (TST, bimolecular reactions) generally utilizing the rigid-rotor, harmonic-oscillator (RRHO) model for the calculations of partition functions for molecular complexes and transition states. Collisional energy transfer rates in the master equation were expressed using the “exponential down” model,<sup>86</sup> with the temperature dependence of the range parameter  $\alpha$  for the deactivating wing of the energy transfer function expressed as  $\alpha(T) = \alpha_{300}(T/300 \text{ K})^n$ , with  $n = 0.86$  and  $\alpha_{300} = 228 \text{ cm}^{-1}$  obtained earlier from classical trajectories calculations as “universal” parameters for hydrocarbons in the nitrogen bath gas.<sup>87</sup> We used the Lennard-Jones parameters ( $\epsilon/\text{cm}^{-1}$ ,  $\sigma/\text{\AA}$ ) = (237, 5.02) for the *n*-decane/nitrogen system derived by Jasper et al.<sup>87</sup> based on the fit of results using the “one-dimensional optimization” method.<sup>88</sup> For  $\beta$ -scission reactions of smaller 1-alkyls we employed Lennard-Jones parameters for the corresponding *n*-alkane/ $N_2$  combinations also derived by Jasper et al.<sup>87</sup>

Two issues are challenging in rate constant calculations, the treatment of barrierless reactions, such as the C–C and C–H single bond cleavages in the original *n*-decane molecule, and the description of multiple (and often coupled) hindered rotors in the molecule and radical products, which possess a large

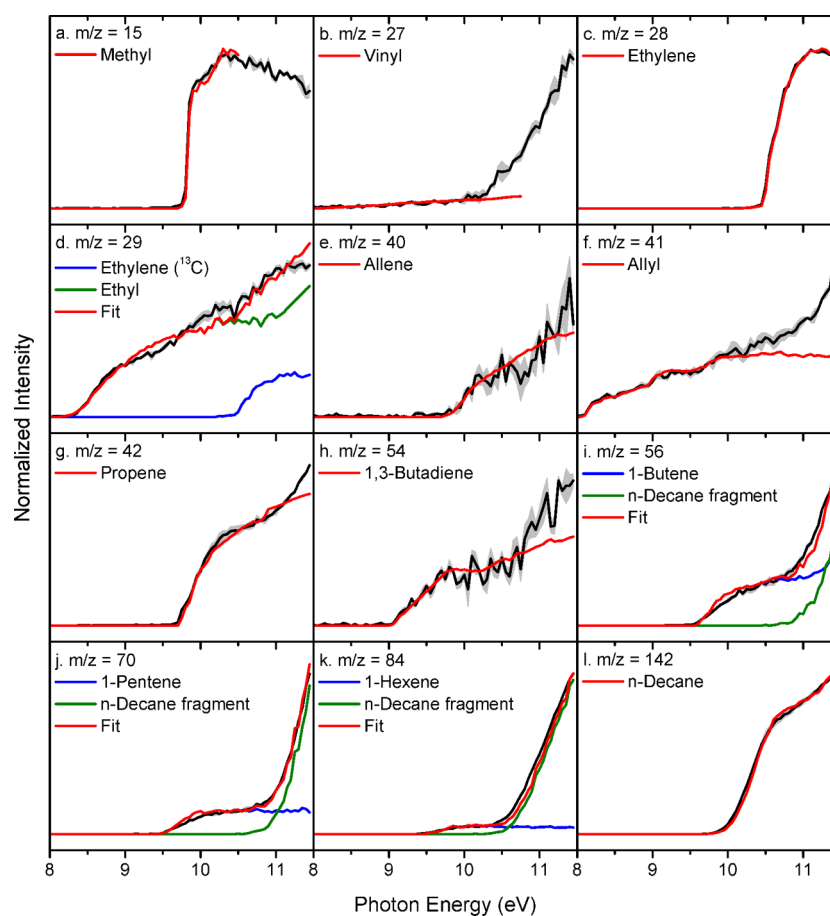


**Figure 5.** Experimental photoionization efficiency curves (PIE, black lines) recorded from the decomposition of *n*-decane at 1300 K along with the experimental errors (gray area), and the reference PIE curves (red, green and blue lines). In the case of multiple contributions to one PIE curve, the red line indicates the sum of contributions. For  $m/z = 41$  and  $54$ , there may be photoionization fragments from products causing the experimental values to be higher than the fitting at higher photon energies.

number of single bonds. Since our goal here is not quantitative prediction of reaction rate constants but rather qualitative evaluation of relative yields of various products at different stages of the pyrolysis in order to account for the observed experimental results, we utilized a number of approximations to address these issues. First, the barrierless single-bond cleavage reactions were treated using phase space theory with the empirical potential energy parameters selected in such a way that the calculated rate constants for the reverse  $C_xH_y + C_{10-x}H_{22-y}$  and  $C_{10}H_{21} + H$  radical recombination reactions reproduce the rate constants for the prototype  $C_2H_5 + C_2H_5$  and  $C_2H_5 + H$  reactions in the experimental 1100–1600 K temperature interval studied earlier by Klippenstein and co-workers<sup>89,90</sup> using the most accurate up-to-date theoretical approach, variable reaction coordinated transition state theory (VRC-TST). Second, the hindered rotor treatment was applied only to smaller  $C_3H_7$  and  $C_4H_9$  radicals while dealing with their  $\beta$ -scission reactions. For these species, soft normal modes were visually examined and those representing internal rotations were considered as one-dimensional hindered rotors in partition function calculations. For larger alkyl radicals,  $C_5H_{11}$ ,  $C_6H_{13}$ ,  $C_7H_{15}$ ,  $C_8H_{17}$ , and  $C_9H_{19}$ , only terminal  $CH_2$ ,  $CH_3$ , and  $C_2H_4$  rotations were treated as hindered rotors, whereas all other convoluted rotations were treated as harmonic oscillators. One-dimensional torsional potentials were calculated by scanning PESs at the B3LYP/6-311G(d,p) level of theory. For comparison, we also performed calculations

of the same rate constants in pure RRHO approximation and found that the replacement of harmonic oscillators with hindered rotors increases the  $\beta$ -scission rate constants by 8–41% at 1000 K, but the difference drops to only 2–25% at 1600 K. For *n*-decane and decyl radicals, visual identification of internal rotations is not practically possible because those are coupled with one another and with other types of motions. Therefore, these species were treated within RRHO keeping in mind the above-mentioned error bars in rate constants. At the same time, the expected errors in ratios of rate constants are expected to be smaller than the errors in their absolute values due to cancelations of similar inaccuracies. Hence we anticipate that the relative product yields are predicted by our calculations with higher accuracy.

#### 4. EXPERIMENTAL RESULTS

Characteristic mass spectra of the products of the pyrolyzed decane precursor ( $C_{10}H_{22}$ ,  $m/z = 142$ ) collected at 10.00 eV photoionization energy are compiled in Figure 2 from 1100 to 1600 K. The data provide evidence of ion counts from mass-to-charge ratios  $m/z = 15$  to 98 along with parent ions of the ionized *n*-decane precursor at  $m/z = 142$ . No ion counts higher than  $m/z = 142$  are observable at any temperature suggesting that mass growth processes under our experimental conditions are absent. This requirement is crucial for the extraction of the initial pyrolysis products of *n*-decane. The newly detected  $m/z$

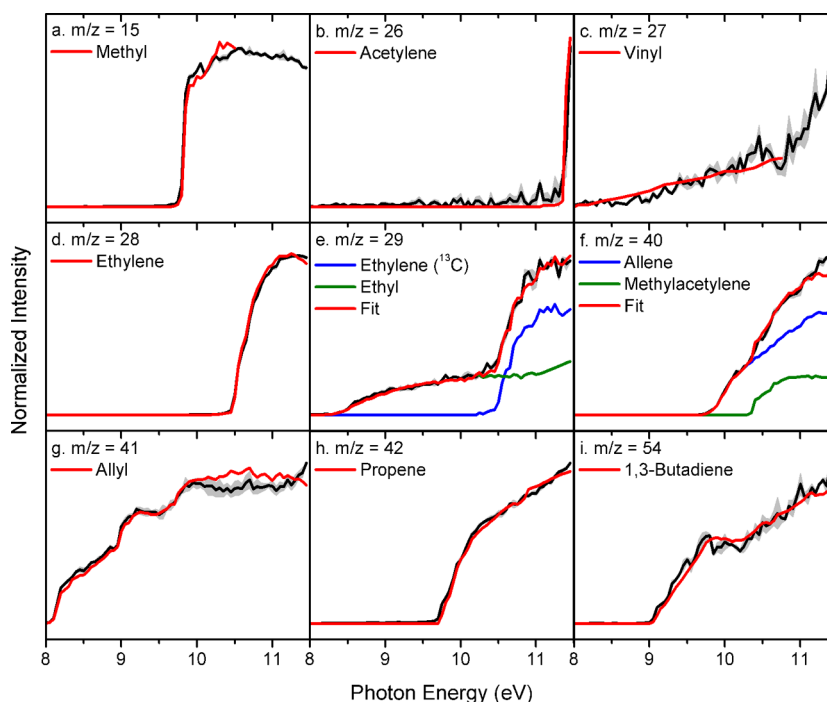


**Figure 6.** Experimental photoionization efficiency (PIE) curves (black lines) recorded from the decomposition of *n*-decane at 1400 K along with the experimental errors (gray area), and the reference PIE curves (red, green, blue and purple lines). In the case of multiple contributions to one PIE curve, the red line resembles indicates the sum of contributions the overall fit.

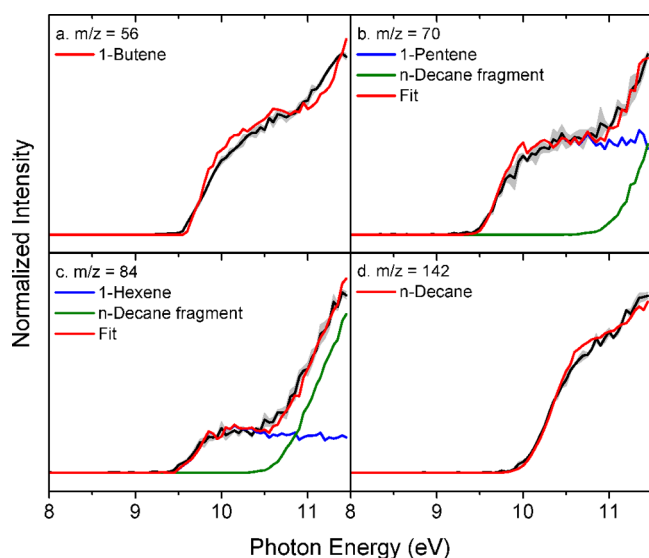


**Figure 7.** Experimental photoionization efficiency (PIE) curves (black lines) recorded from the decomposition of *n*-decane at 1400 K along with the experimental errors (gray area), and the reference PIE curves (red, green, and blue lines). In the case of multiple contributions to one PIE curve, the red line indicates the sum of contributions.

together with the molecular formulas and assignments of the products are listed in Tables 2 and 3; the corresponding PIE curves along with the best fits are visualized in Figures 3–9 for all temperatures between 1100 K and 1600 K. To elucidate the nature of the products formed, the individual PIE curves from  $m/z = 15$  to 142 were fit with (a linear combination of) known PIE curves of the corresponding structural isomers. In all figures, the black line represents the average of the experimental PIE scans; the shaded areas define the experimental uncertainties. The best fits are reported by red lines. If multiple

literature PIE curves were required to fit the experimental data, blue, green and purple lines refer to these individual PIE curves. Literature PIE curves were taken from the photoionization cross section database<sup>78</sup> and are individually referenced. As detailed in the Experimental Approach, the experimentally determined ratios of the ion counts were corrected for the absolute photoionization cross sections as compiled in Table 4. It should be noted that care has to be taken to fit the PIE curves at higher photon energies beyond 10.5 eV, as the photolysis of *n*-decane generates multiple fragment ions via dissociative photoionization of the parent ion; these fragment ions are labeled as *n*-decane fragment in Figures 3–9. The detailed analysis of the temperature dependence of the PIE curves (Figures 3–9) as outlined above reveals interesting results.

- (1) The intensity of the parent ion of *n*-decane ( $m/z = 142$ ) decreases as the temperature rises from 99.6% (1100 K) via 88.7% (1200 K), 63.4% (1300 K), and 3.7% (1400 K) and eventually vanishes at 1500 K. This suggests that the decomposition of the *n*-decane precursor is complete at 1500 K, under these detection conditions.
- (2) As compiled in Table 3, as the temperature increases, the number of pyrolysis products first rises from only three C2 to C4 alkenes (ethylene (C<sub>2</sub>H<sub>4</sub>), propene (C<sub>3</sub>H<sub>6</sub>), 1-butene (C<sub>4</sub>H<sub>8</sub>)) at 1100 K to nine (1200 K), 12 (1300 K), and 15 C1–C6/C1–C4 products (1400, 1500 K) before ultimately decreasing to 11 C1–C4 products (1600 K). This trend suggests that as the temperature increases beyond 1400 K, the enhanced temperature leads to a degradation of the initial higher molecular weight products such as the C5 and C6 hydrocarbons. The mole fractions of the species observed were provided in Table S2 in the Supporting Information.
- (3) We have identified 18 C0 to C7 products, which can be arranged into six groups. (i) a homologues series of

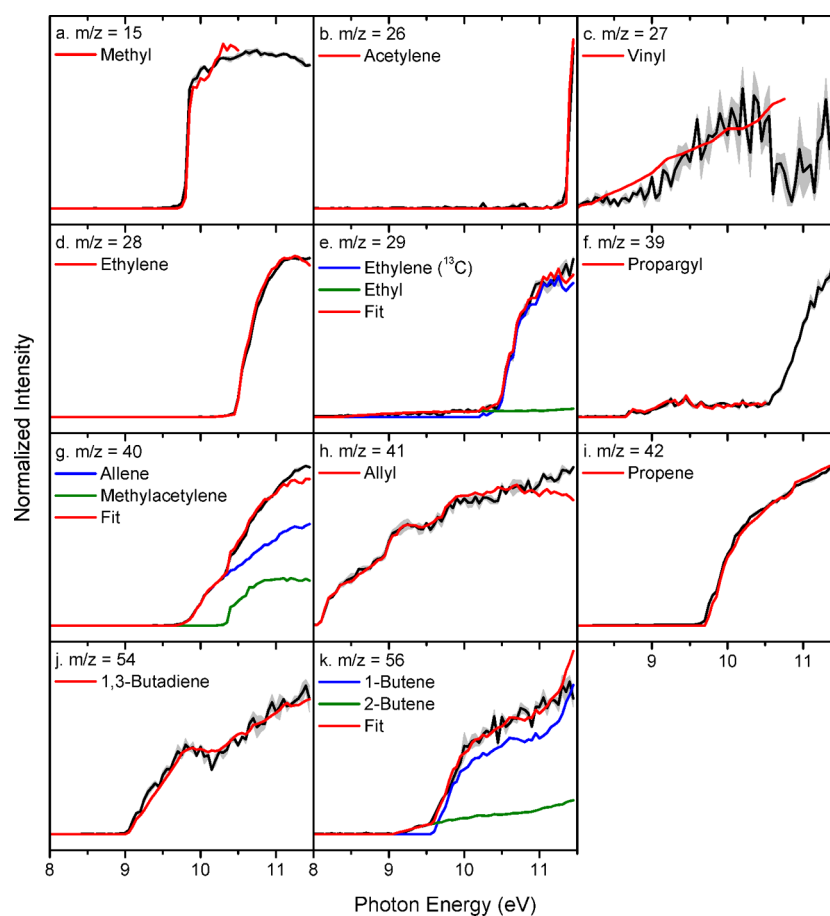


**Figure 8.** Experimental photoionization efficiency (PIE) curves (black lines) recorded from the decomposition of *n*-decane at 1500 K along with the experimental errors (gray area), and the reference PIE curves (red, green, and blue lines). In the case of multiple contributions to one PIE curve, the red line indicates the sum of contributions.

alkenes [C2–C7; ethylene ( $C_2H_4$ ), propene ( $C_3H_6$ ), 1-butene ( $C_4H_8$ ), 2-butene ( $C_4H_8$ ), 1-pentene ( $C_5H_{10}$ ), 1-hexene ( $C_6H_{12}$ ), 1-heptene ( $C_7H_{14}$ )] (ii) diene [1,3-butadiene ( $C_4H_6$ )], (iii) cumulene [allene ( $C_3H_4$ )], (iv) alkynes [acetylene ( $C_2H_2$ ), methylacetylene ( $C_3H_4$ )], (v) radicals [methyl ( $CH_3$ ), vinyl ( $C_2H_3$ ), ethyl ( $C_2H_5$ ), propargyl ( $C_3H_3$ ), allyl ( $C_3H_5$ )], and (vi) smaller products [hydrogen ( $H_2$ ), methane ( $CH_4$ )]. The appearance energies (ionization onsets) of these products as determined in our experiments agree very well with the adiabatic ionization energies as compiled in Table 5 with deviations of typically 0.05 eV in cases of excellent signal-to-noise ratios of the PIE curves, but not more than 0.08 eV. Among these species, it is important to highlight that this technique is ideally suited to detect C1 to C3 radical species as pyrolysis products, among them the vinyl ( $C_2H_3$ ) and the ethyl ( $C_2H_5$ ) radical being detected for the first time in *n*-decane pyrolysis experiments.

- (4) Table 3 and Figure 10 quantify that ethylene ( $C_2H_4$ ) represents the major decomposition products of *n*-decane over the complete temperature range increasing from about 40% to 63% from 1100 K to 1500 K. It is important to highlight that simultaneously the branching ratios of the chemically related ethyl radical ( $C_2H_5$ ) decrease from about 15% at 1200 K to less than 0.2% at 1500 K. In the range of 1200–1500 K, the combined

branching ratios of ethylene and the ethyl radical stay essentially constant with only a slight rise covering about 58% to 63% of the products formed in the pyrolysis of *n*-decane. Both acetylene ( $C_2H_2$ ) and the vinyl radical ( $C_2H_3$ ) represent only minor products of 3% at most (1600 K). Besides these C2 products, propene ( $C_3H_6$ ) with branching ratios decreasing from about 22% (1100 K) to 6% (1600 K) represents the most prominent C3 product. The C3 closed-shell products allene and methylacetylene ( $C_3H_4$ ) along with the C3 radicals propargyl ( $C_3H_3$ ) and allyl ( $C_3H_5$ ) only contribute a total from about 1% (1200 K) to 6% (1500 K) to the total branching ratio before declining to about 3% as the temperature rises to 1600 K. The branching ratios of the C4 to C7 alkenes steadily decrease as the temperature rises from 1100 to 1600 K, suggesting that these alkenes decompose in consecutive processes. Therefore, this trend proposes that the C4 to C7 hydrocarbons can be classified as reaction intermediates. As a matter of fact, at 1500 K, 1-pentene, 1-hexene, and 1-heptene are completely decomposed and hence undetectable. At 1600 K, among the C4 to C7 products, only C4 species including 1,3-butadiene ( $C_4H_6$ ), 1-butene ( $C_4H_8$ ) and 2-butene ( $C_4H_8$ ) survive at fractions of less than 1%. Finally, it should be noted that we detected molecular hydrogen along with the methyl radical ( $CH_3$ ) and methane ( $CH_4$ ). In Figure 10 and Table 3, molecular

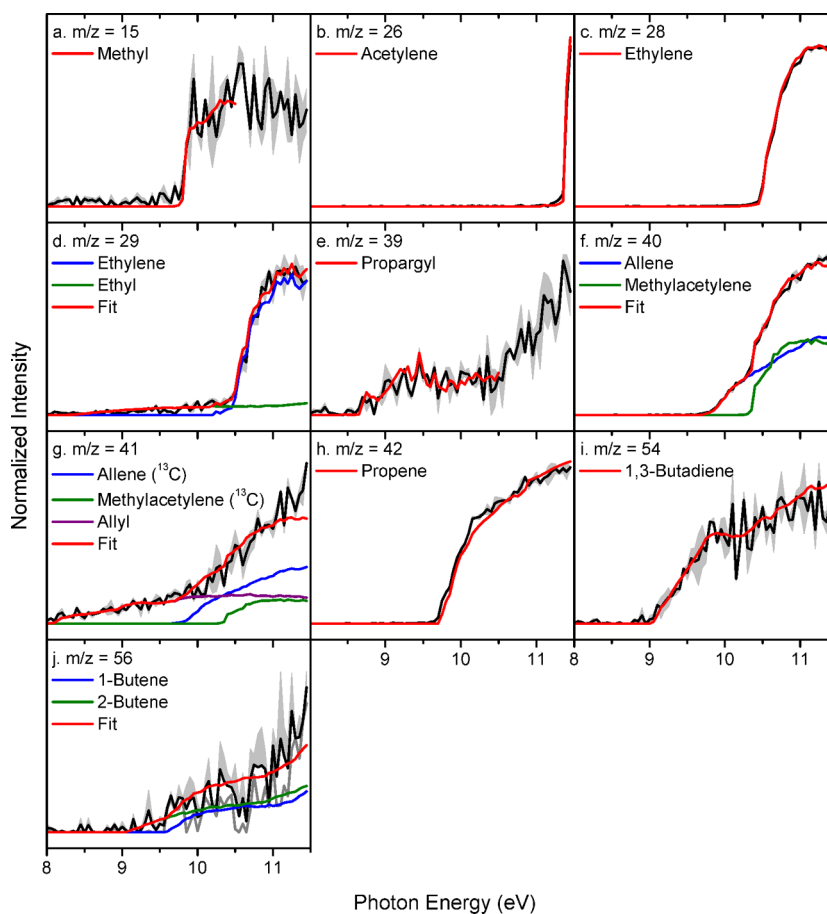


**Figure 9.** Experimental photoionization efficiency (PIE) curves (black lines) recorded from the decomposition of *n*-decane at 1600 K along with the experimental errors (gray area), and the reference PIE curves (red, green, and blue lines). In the case of multiple contributions to one PIE curve, the red line indicates the sum of contributions.

**Table 2.** Compilation of Products Observed in the Present Studies on the Decomposition of *n*-Decane<sup>a</sup>

Species	Formula	Mass	Structure
Hydrogen	H <sub>2</sub>	2	H—H
Methyl radical	CH <sub>3</sub>	15	CH <sub>3</sub> •
Methane	CH <sub>4</sub>	16	CH <sub>4</sub>
Acetylene	C <sub>2</sub> H <sub>2</sub>	26	≡≡
<b>Vinyl radical</b>	C <sub>2</sub> H <sub>3</sub>	27	≡•
Ethylene	C <sub>2</sub> H <sub>4</sub>	28	≡≡
<b>Ethyl radical</b>	C <sub>2</sub> H <sub>5</sub>	29	≡•
Propargyl radical	C <sub>3</sub> H <sub>3</sub>	39	≡•
Allene	C <sub>3</sub> H <sub>4</sub>	40	≡C=C=C
Methylacetylene	C <sub>3</sub> H <sub>4</sub>	40	≡C—CH <sub>3</sub>
Allyl radical	C <sub>3</sub> H <sub>5</sub>	41	≡CH <sub>2</sub> •
Propene	C <sub>3</sub> H <sub>6</sub>	42	≡CH=CH <sub>2</sub>
1,3-Butadiene	C <sub>4</sub> H <sub>6</sub>	54	≡CH=CH=CH <sub>2</sub>
1-Butene	C <sub>4</sub> H <sub>8</sub>	56	≡CH=CH—CH <sub>2</sub> —CH <sub>3</sub>
2-Butene	C <sub>4</sub> H <sub>8</sub>	56	≡CH—CH=CH—CH <sub>3</sub>
1-Pentene	C <sub>5</sub> H <sub>10</sub>	70	≡CH=CH—CH <sub>2</sub> —CH <sub>2</sub> —CH <sub>3</sub>
1-Hexene	C <sub>6</sub> H <sub>12</sub>	84	≡CH=CH—CH <sub>2</sub> —CH <sub>2</sub> —CH <sub>2</sub> —CH <sub>3</sub>
1-Heptene	C <sub>7</sub> H <sub>14</sub>	98	≡CH=CH—CH <sub>2</sub> —CH <sub>2</sub> —CH <sub>2</sub> —CH <sub>2</sub> —CH <sub>3</sub>

<sup>a</sup>Vinyl and ethyl radicals, detected for the first time are highlighted in bold.

**Table 3. Branching Fractions of the Products Observed in the Decomposition of *n*-Decane at 600 Torr in the Chemical Reactor at 1100, 1200, 1300, 1400, 1500, and 1600 K**

species <sup>a</sup>	formula	mass	temperature					
			1100 K	1200 K	1300 K	1400 K	1500 K	1600 K
hydrogen	H <sub>2</sub>	2	–	–	1.05 ± 0.34	1.11 ± 0.28	2.43 ± 0.55	34.15 ± 8.45
methyl radical	CH <sub>3</sub>	15	–	12.88 ± 4.01	16.19 ± 3.79	16.40 ± 3.93	14.66 ± 3.36	0.37 ± 0.08
methane	CH <sub>4</sub>	16	–	–	–	0.07 ± 0.02	0.11 ± 0.02	0.13 ± 0.04
acetylene	C <sub>2</sub> H <sub>2</sub>	26	–	–	–	0.18 ± 0.04	0.61 ± 0.15	2.63 ± 0.54
vinyl radical	C <sub>2</sub> H <sub>3</sub>	27	–	–	0.06 ± 0.02	0.08 ± 0.02	0.07 ± 0.02	–
ethylene	C <sub>2</sub> H <sub>4</sub>	28	40.17 ± 10.57	43.13 ± 9.52	51.99 ± 11.36	60.73 ± 13.67	63.06 ± 13.80	53.00 ± 11.80
ethyl radical	C <sub>2</sub> H <sub>5</sub>	29	–	15.04 ± 3.77	6.63 ± 1.52	1.02 ± 0.26	0.17 ± 0.07	0.20 ± 0.09
propargyl radical	C <sub>3</sub> H <sub>3</sub>	39	–	–	–	–	0.07 ± 0.02	0.03 ± 0.01
allene	C <sub>3</sub> H <sub>4</sub>	40	–	–	0.08 ± 0.05	0.89 ± 0.21	3.03 ± 0.81	1.46 ± 0.47
methylacetylene	C <sub>3</sub> H <sub>4</sub>	40	–	–	–	0.69 ± 0.17	2.61 ± 0.63	1.47 ± 0.32
allyl radical	C <sub>3</sub> H <sub>5</sub>	41	–	0.94 ± 0.19	1.97 ± 0.39	4.60 ± 0.92	2.36 ± 0.47	0.10 ± 0.02
propene	C <sub>3</sub> H <sub>6</sub>	42	22.00 ± 7.89	13.64 ± 3.45	12.56 ± 2.94	10.91 ± 2.54	10.03 ± 2.23	6.32 ± 1.47
1,3-butadiene	C <sub>4</sub> H <sub>6</sub>	54	–	–	0.15 ± 0.04	0.30 ± 0.07	0.35 ± 0.08	0.12 ± 0.03
1-butene	C <sub>4</sub> H <sub>8</sub>	56	37.83 ± 13.04	9.84 ± 2.62	5.22 ± 1.21	2.23 ± 0.50	0.38 ± 0.09	0.03 ± 0.01
2-butene	C <sub>4</sub> H <sub>8</sub>	56	–	–	–	–	0.08 ± 0.03	0.01 ± 0.01
1-pentene	C <sub>5</sub> H <sub>10</sub>	70	–	2.96 ± 0.99	1.89 ± 0.52	0.46 ± 0.12	–	–
1-hexene	C <sub>6</sub> H <sub>12</sub>	84	–	1.57 ± 0.78	2.20 ± 0.53	0.33 ± 0.08	–	–
1-heptene	C <sub>7</sub> H <sub>14</sub>	98	–	0.13 ± 0.03	1.00 ± 0.04	0.09 ± 0.05	–	–

<sup>a</sup>Note: As there is no cross section database of 1-heptene, its branching fraction cannot be calculated. Therefore, the normalized ion count intensities of 1-heptene at 10.0 eV are listed in the last row to reveal the trend of 1-heptene formation from 1100 to 1600 K.

**Table 4. Photoionization Cross Sections (Mb) of the Species at Selected Energies Exploited for the Calculations of the Branching Ratios in This Work**

species	formula	mass	photon energy (eV)						ref
			9.5	10.0	10.5	11.0	11.5	15.5	
hydrogen	H <sub>2</sub>	2	–	–	–	–	–	4.73	105
methyl radical	CH <sub>3</sub>	15	–	4.78	5.81	–	–	–	106
methane	CH <sub>4</sub>	16	–	–	–	–	–	23.87	107
acetylene	C <sub>2</sub> H <sub>2</sub>	26	–	–	–	–	18.258	–	76
vinyl radical	C <sub>2</sub> H <sub>3</sub>	27	8.0425	11.064	13.32	–	–	–	108
ethylene	C <sub>2</sub> H <sub>4</sub>	28	–	–	0.918	7.794	8.016	–	107
ethyl radical	C <sub>2</sub> H <sub>5</sub>	29	4.36	5.05	5.52	5.64	5.37	–	109
propargyl radical	C <sub>3</sub> H <sub>3</sub>	39	26.56	21.09	26.29	–	–	–	106
allene	C <sub>3</sub> H <sub>4</sub>	40	–	5.66	15.48	22.26	25.84	–	110
methylacetylene	C <sub>3</sub> H <sub>4</sub>	40	–	–	23.06	43.84	42.1	–	107
allyl radical	C <sub>3</sub> H <sub>5</sub>	41	5.636	6.227	6.091	–	–	–	111
propene	C <sub>3</sub> H <sub>6</sub>	42	–	5.33	9.05	11.40	12.66	–	112
1,3-butadiene	C <sub>4</sub> H <sub>6</sub>	54	8.48	13.96	16.44	19.91	22.45	–	110
1-butene	C <sub>4</sub> H <sub>8</sub>	56	–	7.35	10.02	10.88	17.33	–	112
2-butene	C <sub>4</sub> H <sub>8</sub>	56	5.24	9.06	11.04	14.05	19.17	–	113
1-pentene	C <sub>5</sub> H <sub>10</sub>	70	0.62	14.38	14.90	14.83	13.92	–	113
1-hexene	C <sub>6</sub> H <sub>12</sub>	84	0.89	8.58	9.65	8.86	9.00	–	110
<i>n</i> -decane	C <sub>10</sub> H <sub>22</sub>	142	0.0025	1.6325	22.2	30.84	37.27	–	55

hydrogen and acetylene present an abrupt increase due to the overheating in the pyrolysis consuming the intermediates to yield the final products.

- (5) The branching ratios as compiled in Table 3 allow us to determine the overall mass balance of the experiments. The overall carbon-to-hydrogen (C/H) ratio is plotted in Figure 11 versus the temperature. The error bars are relatively large due to the photoionization cross section uncertainties of up to 20%.<sup>75</sup> The expected C/H ratio of 0.45 is fully recovered at 1100 K suggesting that the mass balance is conserved; this is likely due to the fact that only three pyrolysis products ethylene (C<sub>2</sub>H<sub>4</sub>), propene (C<sub>3</sub>H<sub>6</sub>) and 1-butene (C<sub>4</sub>H<sub>8</sub>) with well-characterized

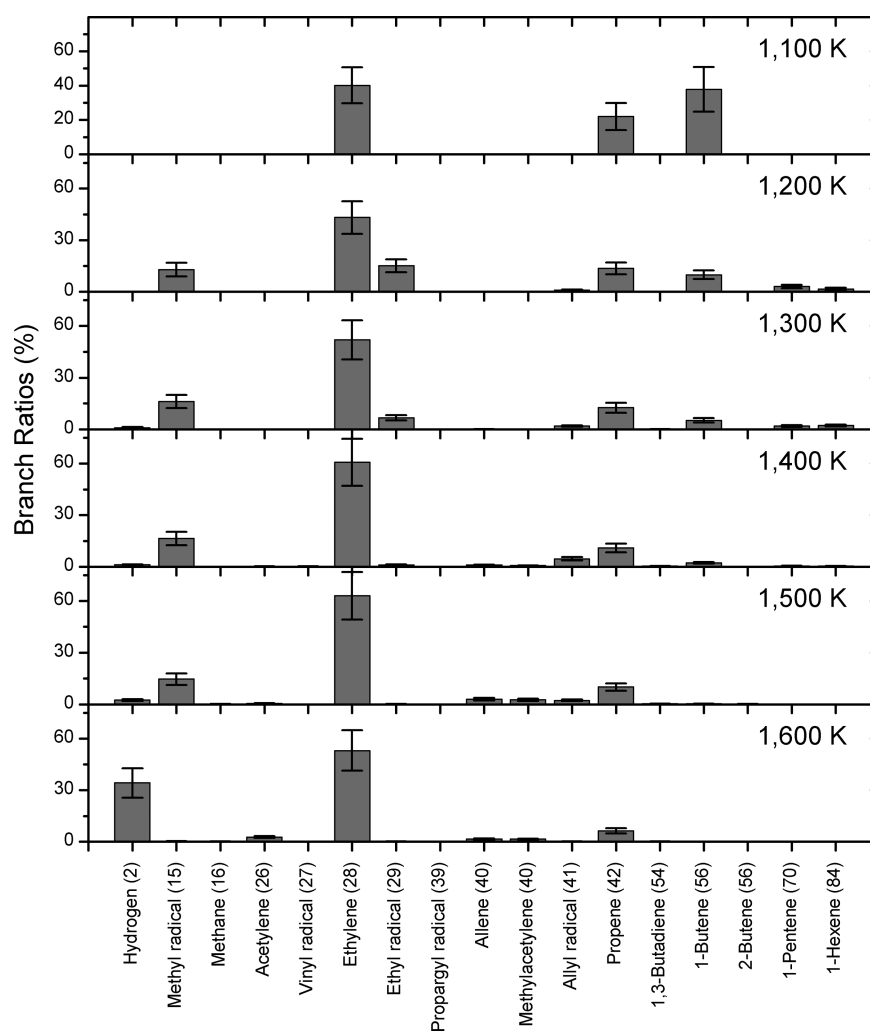
photoionization cross sections are detected (Tables 4 and 5). As the temperature rises, the C/H ratio profile diverges a little from the expected ratio of 0.45, but the error bars still cover the constant line at 0.45 in the whole temperature range.

## 5. COMPUTATIONAL RESULTS

In order to understand the mechanism of *n*-decane pyrolysis and to account for the products observed experimentally, we computed first the potential energy diagrams for the unimolecular decomposition of *n*-decane (C<sub>10</sub>H<sub>22</sub>) along with the primary products. The *n*-decane molecule can break apart

Table 5. Photoionization Energies of the Detected Species in the Present Experiments Compared to Literature Data

species	formula	mass	photoionization energy (eV)						
			database <sup>78</sup>	1100 K	1200 K	1300 K	1400 K	1500 K	1600 K
methyl radical	CH <sub>3</sub>	15	9.839	—	9.75	9.75	9.80	9.75	9.80
acetylene	C <sub>2</sub> H <sub>2</sub>	26	11.4	—	—	—	11.30	11.35	11.35
vinyl radical	C <sub>2</sub> H <sub>3</sub>	27	8.25	—	—	8.20	8.20	8.20	—
ethylene	C <sub>2</sub> H <sub>4</sub>	28	10.514	10.55	10.50	10.45	10.45	10.45	10.45
ethyl radical	C <sub>2</sub> H <sub>5</sub>	29	8.117	—	8.25	8.20	8.20	8.10	8.20
propargyl radical	C <sub>3</sub> H <sub>3</sub>	39	8.67	—	—	—	—	8.70	8.65
allene	C <sub>3</sub> H <sub>4</sub>	40	9.692	—	—	9.75	9.75	9.70	9.70
methylacetylene	C <sub>3</sub> H <sub>4</sub>	40	10.36	—	—	—	10.30	10.30	10.35
allyl radical	C <sub>3</sub> H <sub>5</sub>	41	8.18	—	8.15	8.15	8.15	8.15	8.15
propene	C <sub>3</sub> H <sub>6</sub>	42	9.73	9.75	9.70	9.70	9.70	9.70	9.70
1,3-butadiene	C <sub>4</sub> H <sub>6</sub>	54	9.072	—	—	9.05	9.10	9.05	9.05
1-butene	C <sub>4</sub> H <sub>8</sub>	56	9.55	9.50	9.55	9.60	9.55	9.55	9.55
2-butene	C <sub>4</sub> H <sub>8</sub>	56	9.11	—	—	—	—	9.10	9.10
1-pentene	C <sub>5</sub> H <sub>10</sub>	70	9.49	—	9.50	9.50	9.50	—	—
1-hexene	C <sub>6</sub> H <sub>12</sub>	84	9.44	—	9.40	9.45	9.45	—	—
1-heptene	C <sub>7</sub> H <sub>14</sub>	98	9.27	—	9.25	9.25	9.25	—	—
<i>n</i> -decane	C <sub>10</sub> H <sub>22</sub>	142	9.65	9.70	9.65	9.70	9.70	—	—

Figure 10. Overall branching ratios of the species detected during the decomposition of *n*-decane at temperatures from 1100 to 1600 K.

by initial cleavage of various C–C (reaction R1) and C–H bonds (reaction R2) producing pairs of 1-alkyl radicals and *n*-decyl radicals plus a hydrogen atom, respectively.



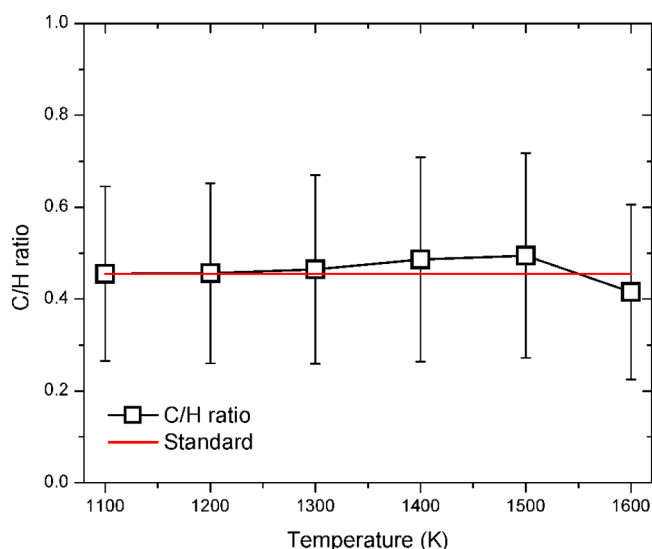


**Figure 11.** Carbon-to-hydrogen (C/H) ratios of the overall decomposition products of *n*-decane in temperatures range from 1100 to 1600 K. The red line indicates the initial C/H ratio of *n*-decane.

**5.1. Homolytic C–C and C–H Bond Cleavages and Consecutive  $\beta$ -Scissions (C–C; C–H).** Let us consider first the C–C bond cleavages as illustrated in Figure 12. The strengths of the C–C bonds are computed to be in the range of 360–368 kJ mol<sup>-1</sup>, with the C2–C3 bond being the weakest and the C4–C5 bond being the strongest. However, the

differences in the C–C bond strengths are rather small and hence it is reasonable to expect that all product pairs, CH<sub>3</sub> + C<sub>9</sub>H<sub>19</sub>, C<sub>2</sub>H<sub>5</sub> + C<sub>8</sub>H<sub>17</sub>, C<sub>3</sub>H<sub>7</sub> + C<sub>7</sub>H<sub>15</sub>, C<sub>4</sub>H<sub>9</sub> + C<sub>6</sub>H<sub>13</sub>, and C<sub>5</sub>H<sub>11</sub> + C<sub>5</sub>H<sub>11</sub>, can be in principle formed. Alternatively, the strengths of C–H bonds appeared to be significantly higher, in the 406–418 kJ mol<sup>-1</sup> range (Figure 12). Here, primary C1–H bonds in terminal CH<sub>3</sub> groups are the strongest and secondary C–H bonds in CH<sub>2</sub> groups vary in a very narrow interval of 406–408 kJ mol<sup>-1</sup>. These results are consistent with the corresponding experimental C–C and C–H bond strengths in *n*-butane, propane, and ethane evaluated based on enthalpies of formation at 0 K from the Active Thermochemical Tables.<sup>91</sup>

This large difference in the bond strengths makes rate constants for the C–H cleavages 4–5 orders of magnitude slower than those for the C–C cleavages and, hence, the cleavage of the C–C bonds is anticipated to be the dominant process in C<sub>10</sub>H<sub>22</sub> unimolecular decomposition (Figure 13a). In the temperature range of 1000–1600 K and 1 atm, the rate constants for the C–C cleavages exhibit well-defined Arrhenius behavior and grow from few s<sup>-1</sup> to 1–2 × 10<sup>6</sup> s<sup>-1</sup>. These values are in accord with the experimental observations that only a small fraction of *n*-decane is consumed at 1100 K, but no parent molecules survive above 1500 K during the residence time, which is tens of microseconds. The computed rates to cleave different C–C bonds are close to each other, and grow to 3–6 × 10<sup>7</sup> s<sup>-1</sup> at 2500 K, except for the one to produce CH<sub>3</sub> + C<sub>9</sub>H<sub>19</sub>, which remains more than an order of magnitude lower. The calculated relative product yields 1.6–1.7% for CH<sub>3</sub> + C<sub>9</sub>H<sub>19</sub>, 37.7–34.1% for C<sub>2</sub>H<sub>5</sub> + C<sub>8</sub>H<sub>17</sub>, 19.1–19.2% for C<sub>3</sub>H<sub>7</sub> + C<sub>7</sub>H<sub>15</sub>, 16.6–18.3% for C<sub>4</sub>H<sub>9</sub> + C<sub>6</sub>H<sub>13</sub>, and 25.0–26.7 for

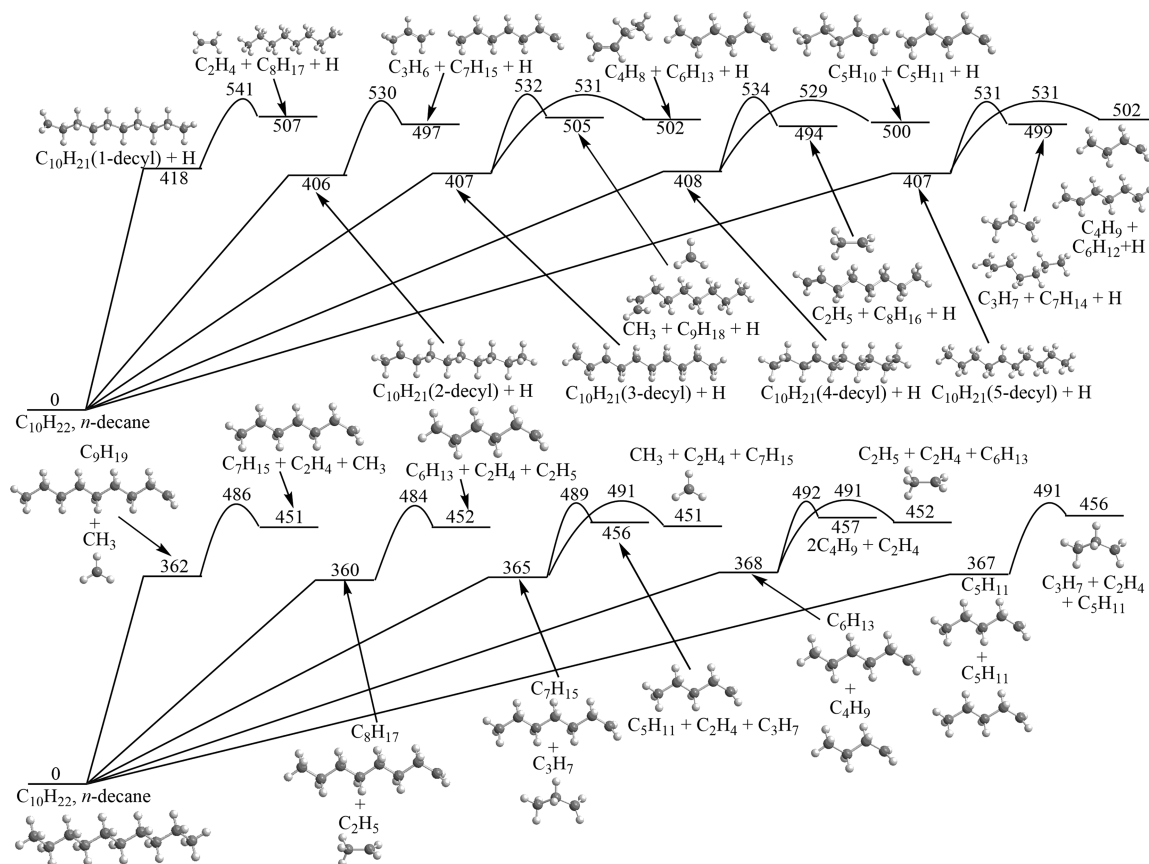


**Figure 12.** Potential energy diagram for primary and secondary dissociation channels of *n*-decane. All relative energies are shown in kJ mol<sup>-1</sup>.

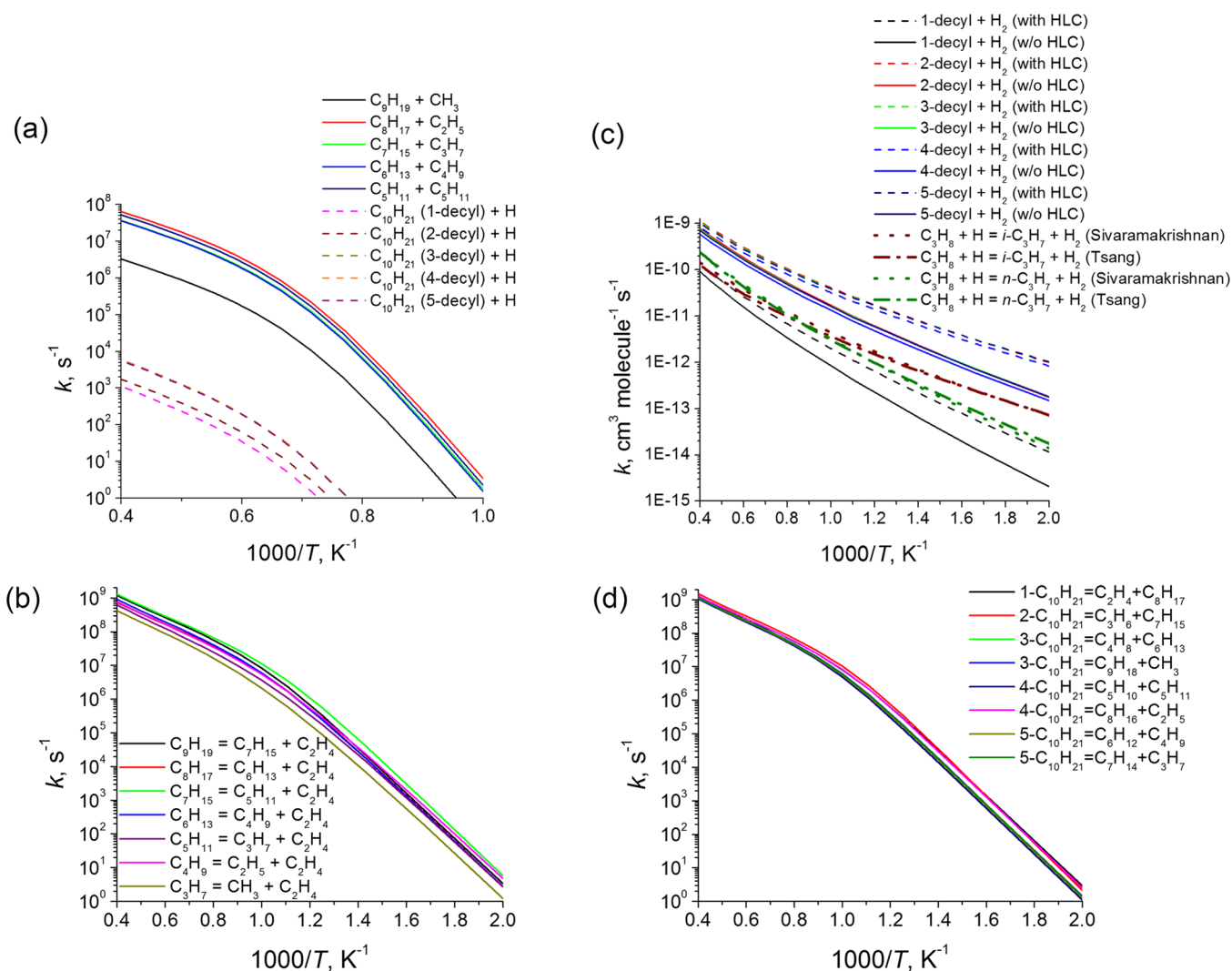
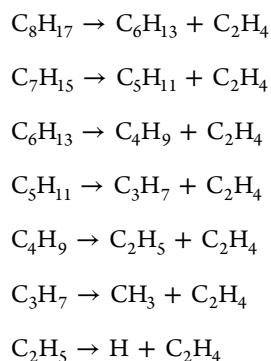


**Figure 13.** Calculated rate constants (at 1 atm for unimolecular reactions): (a) for C–C and C–H bond cleavages in  $\text{C}_{10}\text{H}_{22}$ ; (b) for C–C bond  $\beta$ -scissions in 1-alkyl radicals; (c) for  $\text{C}_{10}\text{H}_{22} + \text{H}$  direct H abstractions; (d) for C–C bond  $\beta$ -scissions in n-decyl radicals  $\text{C}_{10}\text{H}_{21}$  ( $n = 1-5$ ).

$\text{C}_5\text{H}_{11} + \text{C}_5\text{H}_{11}$  in the 1000–1600 K interval, exhibiting only slight temperature dependence up to 2500 K. Calculations at different pressures from 600 Torr to 100 atm show that the product branching ratios are practically independent of pressure. Summarizing, the pyrolysis of *n*-decane at 1500 K and above is predicted to predominantly produce a mixture of 1-alkyl radicals, from ethyl to 1-octyl, on the time scale of 1  $\mu\text{s}$  or less.

The higher 1-alkyl radicals appeared to be unstable at the experimental conditions and are subjected to a rapid C–C bond  $\beta$ -scission producing ethylene  $\text{C}_2\text{H}_4$  in conjunction with a smaller 1-alkyl. As seen in Figure 12 and Table 6, the calculated barrier heights and reaction energies for the C–C bond  $\beta$ -scissions are 123–126 and 86–90  $\text{kJ mol}^{-1}$ , respectively. The computed rate constants for C–C bond  $\beta$ -scissions are approximately in the range of  $10^7$ – $10^8 \text{ s}^{-1}$  in the experimental temperature interval (Figure 13b). Thus, the lifetimes of the primary dissociation products, 1-alkyl radicals, is shorter than 1  $\mu\text{s}$  under the experimental conditions and they are predicted to rapidly decompose forming the ultimate products  $\text{C}_2\text{H}_4$ ,  $\text{CH}_3$ , and  $\text{C}_2\text{H}_5$  as detected experimentally via the stepwise mechanism shown below. The ethyl radical would further lose an H atom via a C–H bond  $\beta$ -scission producing ethylene.



However, this mechanism cannot account for the experimental observation of higher 1-alkenes, especially propene and 1-butene, which are found among major pyrolysis products at 1100 K and are still significant up to 1400 K. One possibility to form 1-alkenes from 1-alkyl radicals is C–H bond  $\beta$ -scission, but the calculations show that C–H  $\beta$ -scission barriers are 20–26  $\text{kJ mol}^{-1}$  higher than the corresponding C–C  $\beta$ -scission barriers in 1-alkyls from  $\text{C}_3\text{H}_7$  to  $\text{C}_8\text{H}_{17}$ . The computed branching ratios for the C–H  $\beta$ -scission channels in  $\text{C}_4\text{H}_9$ – $\text{C}_8\text{H}_{17}$  are very small and do not exceed 1–2% until the highest temperatures and pressures (2,500 K and 100 atm), where they

**Table 6.** Calculated Barrier Heights and Reaction Energies for Various C–C Bond  $\beta$ -Scission and Direct H Abstraction Reactions

reaction	barrier (kJ mol <sup>-1</sup> )	reaction energy (kJ mol <sup>-1</sup> )
C <sub>9</sub> H <sub>19</sub> → C <sub>7</sub> H <sub>15</sub> + C <sub>2</sub> H <sub>4</sub>	124	89
C <sub>8</sub> H <sub>17</sub> → C <sub>6</sub> H <sub>13</sub> + C <sub>2</sub> H <sub>4</sub>	124	92
C <sub>7</sub> H <sub>15</sub> → C <sub>5</sub> H <sub>11</sub> + C <sub>2</sub> H <sub>4</sub>	124	91
C <sub>6</sub> H <sub>13</sub> → C <sub>4</sub> H <sub>9</sub> + C <sub>2</sub> H <sub>4</sub>	124	89
C <sub>5</sub> H <sub>11</sub> → C <sub>3</sub> H <sub>7</sub> + C <sub>2</sub> H <sub>4</sub>	124	89
C <sub>4</sub> H <sub>9</sub> → C <sub>2</sub> H <sub>5</sub> + C <sub>2</sub> H <sub>4</sub>	123	86
C <sub>3</sub> H <sub>7</sub> → CH <sub>3</sub> + C <sub>2</sub> H <sub>4</sub>	126	86
C <sub>10</sub> H <sub>21</sub> (1-decyl) → C <sub>8</sub> H <sub>17</sub> + C <sub>2</sub> H <sub>4</sub>	123	89
C <sub>10</sub> H <sub>21</sub> (2-decyl) → C <sub>7</sub> H <sub>15</sub> + C <sub>3</sub> H <sub>6</sub>	124	91
C <sub>10</sub> H <sub>21</sub> (3-decyl) → C <sub>9</sub> H <sub>18</sub> + CH <sub>3</sub>	125	98
C <sub>10</sub> H <sub>21</sub> (3-decyl) → C <sub>6</sub> H <sub>13</sub> + C <sub>4</sub> H <sub>8</sub>	124	95
C <sub>10</sub> H <sub>21</sub> (4-decyl) → C <sub>8</sub> H <sub>16</sub> + C <sub>2</sub> H <sub>5</sub>	126	86
C <sub>10</sub> H <sub>21</sub> (4-decyl) → C <sub>5</sub> H <sub>10</sub> + C <sub>5</sub> H <sub>11</sub>	121	92
C <sub>10</sub> H <sub>21</sub> (5-decyl) → C <sub>7</sub> H <sub>14</sub> + C <sub>3</sub> H <sub>7</sub>	124	95
C <sub>10</sub> H <sub>21</sub> (5-decyl) → C <sub>6</sub> H <sub>12</sub> + C <sub>4</sub> H <sub>9</sub>	124	92
C <sub>10</sub> H <sub>22</sub> + H → C <sub>10</sub> H <sub>21</sub> (1-decyl) + H <sub>2</sub>	47 (40) <sup>a</sup>	-12 (-19) <sup>a</sup>
C <sub>10</sub> H <sub>22</sub> + H → C <sub>10</sub> H <sub>21</sub> (2-decyl) + H <sub>2</sub>	34 (26) <sup>a</sup>	-24 (-31) <sup>a</sup>
C <sub>10</sub> H <sub>22</sub> + H → C <sub>10</sub> H <sub>21</sub> (3-decyl) + H <sub>2</sub>	33 (26) <sup>a</sup>	-23 (-31) <sup>a</sup>
C <sub>10</sub> H <sub>22</sub> + H → C <sub>10</sub> H <sub>21</sub> (4-decyl) + H <sub>2</sub>	33 (26) <sup>a</sup>	-23 (-30) <sup>a</sup>
C <sub>10</sub> H <sub>22</sub> + H → C <sub>10</sub> H <sub>21</sub> (5-decyl) + H <sub>2</sub>	33 (26) <sup>a</sup>	-23 (-30) <sup>a</sup>

<sup>a</sup>The values including the higher level correction (HLC) for H abstractions are given in parentheses.

reach 5–6% (Tables S3–S6; Supporting Information). The relative yield of propene + H is higher from the *n*-propyl radical (C<sub>3</sub>H<sub>7</sub>) and constitutes 3–4% at 1100–1600 K and 1 atm increasing to 6%, 9%, and 13% at 2500 K and pressures of 1, 10, and 100 atm, respectively. Thus, C–H bond  $\beta$ -scissions cannot explain the large experimental yields of propene and 1-butene at low temperatures since they are unfavorable compared to the  $\beta$ -scissions involving loss of ethylene (C<sub>2</sub>H<sub>4</sub>). In summary, C–C bond cleavages leading to 1-alkyl radicals are strongly favored compared to C–H bond rupture processes; the higher 1-alkyl radicals (>C<sub>2</sub>) do not survive under our experimental conditions and decay via successive C–C  $\beta$ -scissions (C<sub>2</sub>H<sub>4</sub> elimination), which dominate over C–H  $\beta$ -scission (alkene formation), to yield eventually the C1 to C2 hydrocarbons methyl (CH<sub>3</sub>), ethyl, (C<sub>2</sub>H<sub>5</sub>), and ethylene (C<sub>2</sub>H<sub>4</sub>).

**5.2. Hydrogen Migrations and Consecutive  $\beta$ -Scissions.** Can the 1-alkyl radicals isomerize before they decompose by C–C bond  $\beta$ -scission? Isomerization channels involving 1,2- and 1,3-H atom shifts in C<sub>3</sub>H<sub>7</sub> and C<sub>4</sub>H<sub>9</sub> are not competitive because the corresponding hydrogen migration barriers are 157–162 kJ mol<sup>-1</sup>, i.e., much higher than the C–C bond  $\beta$ -scission barriers. However, in higher 1-alkyl radicals, beginning from C<sub>5</sub>H<sub>11</sub>, a possibility of 1,4-H, 1,5-H, 1,6-H, and 1,7-H shifts eventually opens up (Figure 14). For instance, 1-pentyl can isomerize to 2-pentyl via a 1,4-H shift, 1-hexyl can isomerize to 2-hexyl and 3-hexyl via 1,5-H and 1,4-H shifts, respectively, 1-heptyl can rearrange to 2-, 3-, and 4-heptyls via 1,6-H, 1,5-H, and 1,4-H shifts, respectively, and 1-octyl can isomerize to 2-, 3-, and 4-octyls via 1,7-H, 1,6-H, and 1,5-H or 1,4-H shifts, respectively. Typical calculated barrier heights for

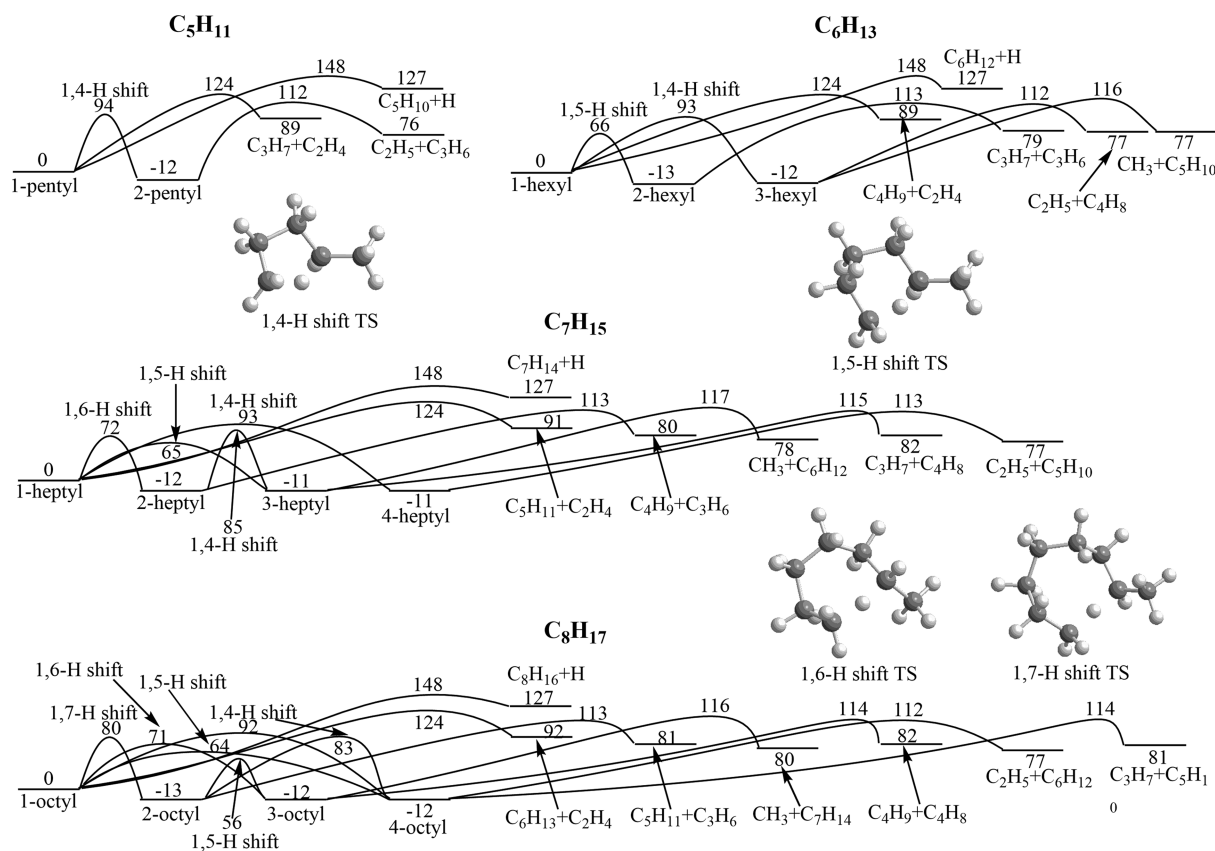


**Figure 14.** Potential energy diagrams for decomposition pathways of C<sub>5</sub>H<sub>11</sub>, C<sub>6</sub>H<sub>13</sub>, C<sub>7</sub>H<sub>15</sub>, and C<sub>8</sub>H<sub>17</sub> involving H shifts and C–C bond  $\beta$ -scissions. All relative energies are given in kJ mol<sup>-1</sup>. Typical structures of transition states for 1,4-, 1,5-, 1,6-, and 1,7-H shifts are also shown.

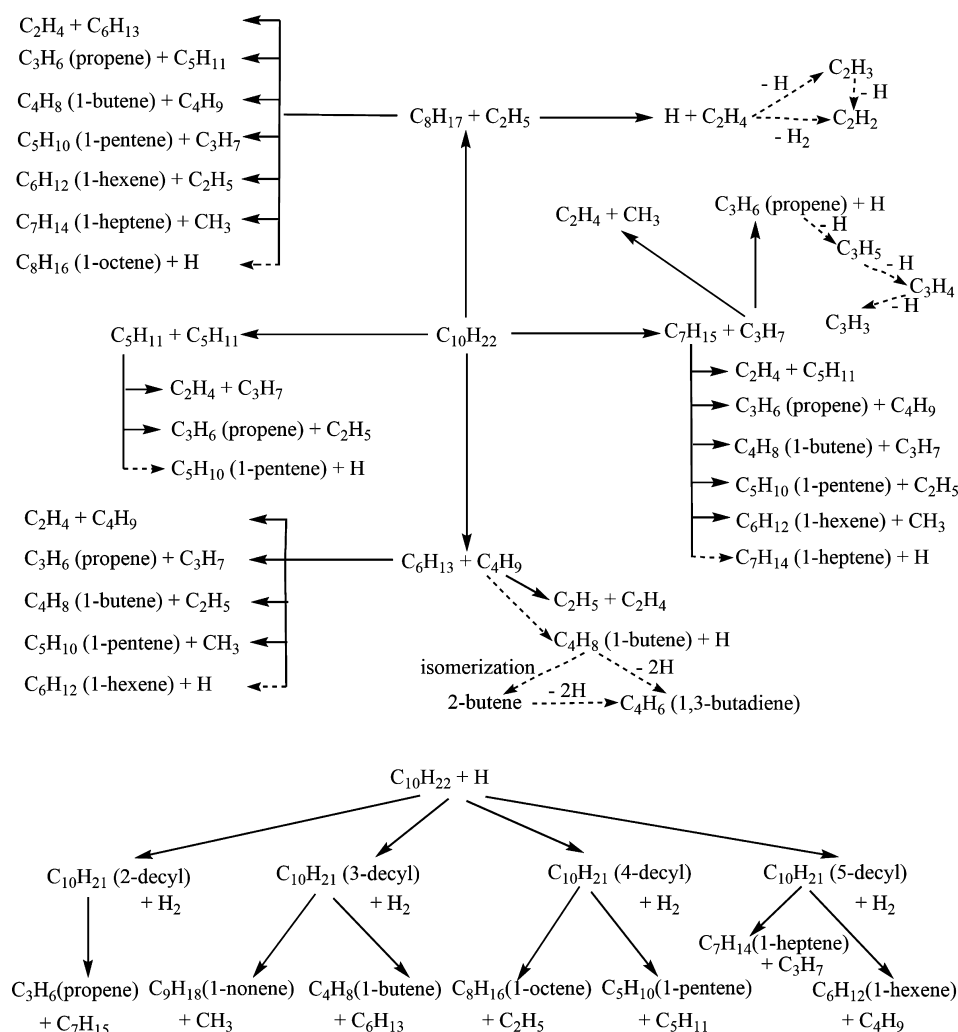
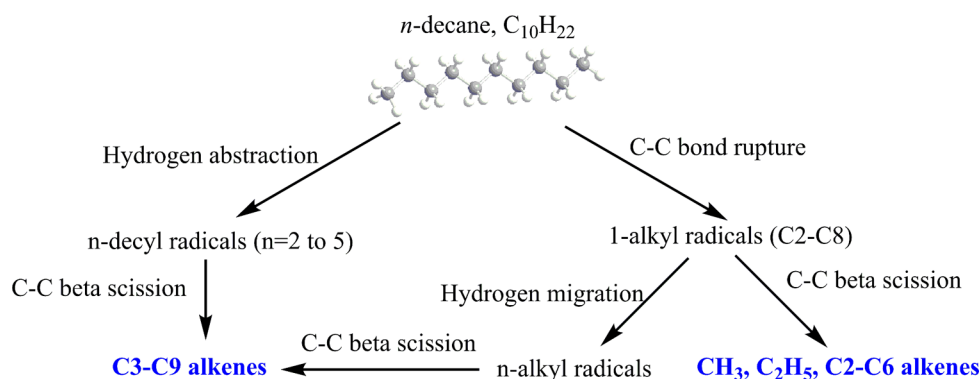


Figure 15. Compiled reaction mechanism for the pyrolysis of *n*-decane.

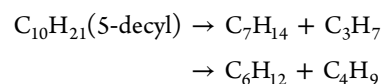
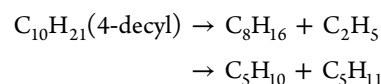
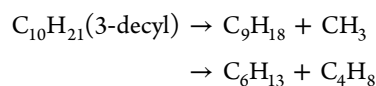
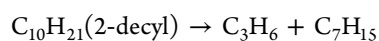
1,4-, 1,5-, 1,6-, and 1,7-H shifts are 92–94, 64–66, 71–72, and 80 kJ mol<sup>-1</sup> and thus they are lower than that for the C–C bond  $\beta$ -scission of about 124 kJ mol<sup>-1</sup>. These hydrogen shifts are followed by C–C  $\beta$ -scissions forming higher 1-alkenes rather than ethylene. For example, 2-pentyl dissociates to propene + C<sub>2</sub>H<sub>5</sub>, 3-hexyl decomposes to either 1-butene + C<sub>2</sub>H<sub>5</sub> or 1-pentene + CH<sub>3</sub>. The C–C  $\beta$ -scission barriers in *n*-alkyls (*n* > 1) exhibit similar heights to those in 1-alkyls and hence all C–C  $\beta$ -scission channels are competitive. The calculated branching ratios presented in Tables S3–S6 of Supporting Information show large dependence on temperature and pressure. Qualitatively, at low pressures up to 1 atm, the products formed following a 1,5-H shift are preferable, but at high pressures of 10 and 100 atm the direct C–C  $\beta$ -scission from 1-alkyls producing ethylene (C<sub>2</sub>H<sub>4</sub>) dominates. Earlier, similar isomerization channels involving H shifts followed by C–C  $\beta$ -scissions producing higher 1-alkenes were proposed by Tsang and co-workers for 1-hexyl<sup>92</sup> and 1-octyl<sup>93</sup> radicals. They derived high-pressure limit rate constants for decomposition and isomerization of hexyl and octyl radicals from shock tube measurements in the ~850–1000 K temperature range and then deduced the pressure dependence from a semiempirical RKKM-ME analysis. A comparison of the present high-pressure limit rate constants (see Table S7) with those proposed by Tsang et al. shows general agreement within a factor or 2 or

better in the experimental temperature range for various  $\beta$ -scission processes. However, deviations are found to be higher for the H shift reactions, for which the present calculations can overestimate the results reported by Tsang et al. by up to a factor of 5. A direct comparison of the branching ratios of various alkenes measured by Tsang et al. in the shock tube experiments from 1-hexyl and 1-octyl is not warranted due to the fast secondary reactions decomposing smaller alkyl radicals; the branching ratios shown in Tables S3–S6 are computed only for the primary decomposition. Clearly, detailed kinetic modeling, which can utilize the rate constants derived here (Table S7), would be required for better description of the experimental data both in the shock tubes and in the pyrolytic reactor, but this is beyond the scope of the present work. In summary, the reaction mechanism involving hydrogen migration in C5 to C8 1-alkyl radicals preceding C–C  $\beta$ -scission accounts for the observation of C3–C7 alkenes [propene, 1-butene, 1-pentene, 1-hexene, and 1-heptene] as monitored in our experiments, and especially, for the large branching ratios of C<sub>3</sub>H<sub>6</sub> and C<sub>4</sub>H<sub>8</sub> at low temperatures. At temperatures of 1500 K and above the lifetime of a single C–C bond approaches 1  $\mu$ s and hence higher alkenes are likely to decompose on the time scale of the experiment and their yield becomes insignificant.



**Figure 16.** Summary of global reaction mechanisms leading to primary reaction products in the decomposition of *n*-decane.

**5.3. Hydrogen Abstraction.** The higher alkenes can be also produced by C–C bond  $\beta$ -scissions in *n*-decyl radicals ( $n > 1$ , see Figure 12 and Table 6). While *n*-decyls are unlikely to be formed by C–H bond cleavages in *n*-decane, they can be produced by direct hydrogen abstractions by hydrogen atoms or other radicals in the reactive system when such radicals become available. The calculated barrier heights and reaction exoergicities for the hydrogen abstraction reactions by hydrogen from secondary C–H bonds are  $\sim 33$  (26) and 23–24 (30–31)  $\text{kJ mol}^{-1}$ , where the values in parentheses include the HLC correction in the G3(CCSD,MP2) calculations. The hydrogen abstractions from the primary C–H bonds are less favorable exhibiting the barrier and the reaction exothermicity of 47 and 12  $\text{kJ mol}^{-1}$ , respectively. The most accurate up-to-date calculations of hydrogen abstraction from  $\text{C}_3\text{H}_8$  and  $\text{C}_2\text{H}_6$  gave the reaction barriers and exoergicities as 32 and 27  $\text{kJ mol}^{-1}$ , respectively, for the secondary hydrogen abstraction, and 43–44 and 15–16  $\text{kJ mol}^{-1}$  for the primary hydrogen abstraction.<sup>94</sup> The calculated rate constants for secondary hydrogen abstractions are similar to each other and are much higher than those for the primary hydrogen abstraction indicating that the most likely products are 2-, 3-, 4- and 5-decyl radicals (Figure 13c). It is noteworthy that the rate constants for secondary hydrogen abstractions evaluated here agree best with the literature data (the most accurate calculations for  $\text{C}_3\text{H}_8$ <sup>94</sup> and experimental data for  $\text{C}_3\text{H}_8$ ,  $\text{C}_4\text{H}_{10}$ , and  $\text{C}_5\text{H}_{12}$ <sup>95,96</sup>) if the HLC correction is not taken into account, but for the primary hydrogen abstraction the agreement is better with the HLC correction. Still, the calculated rate constants for  $\text{C}_{10}\text{H}_{22} + \text{H}$  secondary hydrogen abstractions overestimate the literature values for  $\text{C}_3\text{H}_8$  from by factors of 2–2.5 at 500 K to factors 4–5 at 2500 K. For the primary hydrogen abstraction, the deviation is smaller and the  $\text{C}_{10}\text{H}_{22} + \text{H}$  rate constants underestimate those for  $\text{C}_3\text{H}_8 + \text{H}$  by 20–50%. Apparently, a more rigorous anharmonic treatment of soft normal modes is required to generate more accurate hydrogen abstraction rate constants but this is beyond our goals in the present work. Here, our main conclusion that the secondary H abstractions are feasible and form *n*-decyl radicals ( $n > 1$ ) with roughly equal yields. Once the *n*-decyl radicals are produced, they can rapidly undergo C–C bond  $\beta$ -scission to yield higher alkenes together with 1-alkyl radicals:



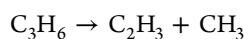
The calculated barriers for these reactions are in the range of 121–126  $\text{kJ mol}^{-1}$  and they are endoergic by 89–98  $\text{kJ mol}^{-1}$ ; the energetic parameters are thus similar as those for C–C  $\beta$ -scissions in smaller alkyl radicals considered above. The rate constants calculated at 1 atm are close for all the reactions considered and indicate that the lifetime of the decyl radicals decreases from 0.1 to 0.2  $\mu\text{s}$  at 1000 K to 3–5 ns at 1600 K (Figure 14d). In summary, *n*-decyl radicals, which may be produced by hydrogen abstraction, can also undergo subsequent C–C bond  $\beta$ -scissions leading to experimentally observed alkenes: 1-butene, 1-pentene, 1-hexene, and 1-heptene.

## 6. DISCUSSION AND CONCLUSION

We combine now the experimental results with the electronic structure and rate constant calculations in an attempt to elucidate the (dominating) temperature-dependent decomposition pathways. The compiled mechanism of the pyrolysis is illustrated in Figures 15 and 16.

- At the initial stage, *n*-decane decomposes by C–C bond cleavages (excluding the terminal C–C bonds) and produces  $\text{C}_8\text{H}_{17} + \text{C}_2\text{H}_5$ ,  $\text{C}_7\text{H}_{15} + \text{C}_3\text{H}_7$ ,  $\text{C}_6\text{H}_{13} + \text{C}_4\text{H}_9$ , and  $\text{C}_5\text{H}_{11} + \text{C}_5\text{H}_{11}$ , i.e., a mixture of C2 to C8 1-alkyl radicals from ethyl to octyl.
- These alkyl radicals are unstable under the experimental conditions. They rapidly dissociate by two possible mechanisms: (a) C–C bond  $\beta$ -scissions to split ethylene ( $\text{C}_2\text{H}_4$ ) plus a 1-alkyl radical with the number of carbon atoms reduced by two and (b) 1,4-, 1,5-, 1,6-, or 1,7-H shifts followed by C–C  $\beta$ -scission producing alkenes from propene to 1-heptene in combination with smaller 1-alkyl radicals. The higher alkenes become increasingly unstable as the temperatures rises and the yield of propene and 1-butene, large at 1100 K, decreases. When the C–C  $\beta$ -scission continues all the way to the propyl radical,  $\text{C}_3\text{H}_7$ , it dissociates producing  $\text{CH}_3 + \text{C}_2\text{H}_4$ . This mechanism allows us to explain the appearance of the predominant pyrolysis products,  $\text{C}_2\text{H}_4$ ,  $\text{CH}_3$ ,  $\text{C}_2\text{H}_5$ ,  $\text{C}_3\text{H}_6$ , and  $\text{C}_4\text{H}_8$  (1-butene), as well as small yields of

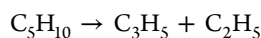
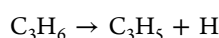
- $C_5H_{10}$  (1-pentene),  $C_6H_{12}$  (1-hexene), and  $C_7H_{14}$  (1-heptene).
- 3 At higher temperatures, hydrogen atoms can abstract hydrogen from  $C_{10}H_{22}$  to yield *n*-decyl radicals, while methyl ( $CH_3$ ) can also abstract hydrogen or recombine with hydrogen to form methane. These *n*-decyl radicals can decompose via C–C-bond  $\beta$ -scissions to C3 to C9 alkenes. Hydrogen migration and  $\beta$ -scissions of radicals are important reactions in hydrocarbon decomposition.<sup>97,98</sup>
- 4 The remaining trace products, which account for a maximum of about 10%, can only be formed via higher-order reactions. In particular, the vinyl radical ( $C_2H_3$ ) and acetylene ( $C_2H_2$ ) can be produced via unimolecular decomposition of ethylene via sequential losses of atomic or molecular hydrogen elimination.<sup>99</sup> Alternatively, vinyl can originate from C–C single bond cleavage in higher alkenes:



or be formed by C–C  $\beta$ -scission in the radicals produced by the C–C bond cleavage in the alkenes:



The allyl radical ( $C_3H_5$ ) can be formed by the primary C–H bond cleavage in propene or a single C–C bond cleavage in higher alkenes. Here, the allyl radical is well-known to eventually decompose to allene ( $C_3H_4$ ), methylacetylene ( $C_3H_4$ ) and the propargyl radical ( $C_3H_3$ ).<sup>100–102</sup>



Finally, 2-butene can be formed by isomerization of 1-butene,<sup>103</sup> whereas 1,3-butadiene is a major dissociation product of the  $C_4H_7$  radical<sup>104</sup> which in turn can be produced by C–H bond cleavage in 1-butene<sup>103</sup> or by C–C bond cleavage in higher alkenes beginning from 1-pentene. Qi et al.<sup>39</sup> outlined that *n*-decane initially decomposed via C–C cleavage followed by  $\beta$ -scission of the C3–C9 radicals. Also, *n*-decane could be consumed by H-abstraction and subsequently produce smaller alkenes. These conclusions agree well with our results.

It is important to place these findings in broader context and in particular to compare those results with previous experimental studies on the decomposition of decane (Table S1). *First*, previous investigations provided important information on the synthesis of closed-shell hydrocarbon intermediates and products as derived mainly from off-line and *ex situ* (HPLC, GC MS) analysis of the decomposition products. This limits the detection of thermally unstable intermediates as well as hydrocarbon radicals in previous studies. On the other hand,

the present investigation to photoionize the decomposition products online and *in situ* presents a unique approach to provide for the first time a complete set of decomposition products including thermally stable and also unstable products (radicals). Recall that photoionization represents a versatile tool to ionize decomposition products. *Second*, we explored the decomposition products on the microsecond time scale, i.e., the initial decomposition products. Previous experiments (Table 1) have experimental time scales in the order of a few milliseconds; this extended time scale is very unfavorable for thermally unstable products and in particular for radicals; this means that although hydrocarbon radicals are initially formed, they do not all survive on the millisecond time scale in the reactors and shock tubes (Table 1). Therefore, the present investigation provides a complete inventory of radicals formed in the initial stage of decomposition, which de facto supply the radical pool for further oxidation of the fuel. *Third*, the short residence time in the present experiments also excludes undesired mass growth processes. This work presents a template of further investigations on the decomposition of JP-8 surrogates and also related to real jet fuel such as JP-10.

## ■ ASSOCIATED CONTENT

### 📄 Supporting Information

The Supporting Information is available free of charge on the ACS Publications website at DOI: 10.1021/acs.jpca.6b11472.

Table S1, detected molecules in previous experimental studies of *n*-decane pyrolysis; Table S2, Mole fractions of the species observed in the decomposition of *n*-decane; Table S3, product branching ratios for dissociation of  $C_5H_{11}$  calculated at various temperatures and pressures within RRHO approximation; Table S4, product branching ratios for dissociation of  $C_6H_{13}$  calculated at various temperatures and pressures within RRHO approximation; Table S5, product branching ratios for dissociation of  $C_7H_{15}$  (1-heptyl radical) calculated at various temperatures and pressures within RRHO approximation; Table S6, product branching ratios for dissociation of  $C_8H_{17}$  calculated at various temperatures and pressures within RRHO approximation; and Table S7, parameters of the fitted modified Arrhenius expressions for most important reactions involved in pyrolysis of *n*-decane (PDF)

## ■ AUTHOR INFORMATION

### Corresponding Authors

\*(R.I.K.) E-mail: ralfk@hawaii.edu.

\*(M.A.) E-mail: MAhmed@lbl.gov.

\*(A.M.M.) E-mail: mebel@fiu.edu.

### ORCID

Tao Yang: 0000-0003-4101-2385

Ralf I. Kaiser: 0000-0002-7233-7206

Alexander M. Mebel: 0000-0002-7233-3133

### Notes

The authors declare no competing financial interest.

## ■ ACKNOWLEDGMENTS

This project is supported by the Air Force Office of Scientific Research (AFOSR) under Grant Number FA9550-15-1-0011 to the University of Hawaii and Florida International University. The work of M.A. and T.P.T. work and the

Advanced Light Source are supported by the Director, Office of Science, Office of Basic Energy Sciences, of the U.S. Department of Energy under Contract No. DE-AC02-05CH11231, through the Chemical Sciences Division. J.M.R. thanks FIU Graduate School for his Doctoral Evidence Acquisition Fellowship.

## REFERENCES

- (1) Bruno, T. J.; Abel, K. R.; Riggs, J. R. Comparison of JP-8 and JP-8 + 100 With the Advanced Distillation Curve Approach. *Energy Fuels* **2012**, *26*, 5843–5850.
- (2) Bezaire, N.; Wadumesthrige, K.; Simon Ng, K. Y.; Salley, S. O. Limitations of the Use of Cetane Index for Alternative Compression Ignition Engine Fuels. *Fuel* **2010**, *89*, 3807–3813.
- (3) Gregg, S. D.; Campbell, J. L.; Fisher, J. W.; Bartlett, M. G. Methods for the Characterization of Jet Propellant-8: Vapor and Aerosol. *Biomed. Chromatogr.* **2007**, *21*, 463–472.
- (4) Gough, R. V.; Bruno, T. J. Composition-Explicit Distillation Curves of Alternative Turbine Fuels. *Energy Fuels* **2013**, *27*, 294–302.
- (5) Meylemans, H. A.; Baldwin, L. C.; Harvey, B. G. Low-Temperature Properties of Renewable High-Density Fuel Blends. *Energy Fuels* **2013**, *27*, 883–888.
- (6) Witten, M. L.; Zeiger, E.; Ritchie, G. D. *Jet Fuel Toxicology*; CRC Press: 2011.
- (7) Rodgers, R. P.; Blumer, E. N.; Freitas, M. A.; Marshall, A. G. Jet Fuel Chemical Composition, Weathering, and Identification as a Contaminant at a Remediation Site, Determined by Fourier Transform Ion Cyclotron Resonance Mass Spectrometry. *Anal. Chem.* **1999**, *71*, 5171–5176.
- (8) DuBois, T. G.; Nieh, S. In *Effects of Hydrocarbon Chemical Class Composition on Autothermal Reforming of JP-8 Fuel*; Power Sources Conference: Las Vegas, NV, Jun. 14–17, 2010.
- (9) Echavarría, C. A.; Jaramillo, I. C.; Sarofim, A. F.; Lighty, J. S. Burnout of Soot Particles in a Two-Stage Burner with a JP-8 Surrogate Fuel. *Combust. Flame* **2012**, *159*, 2441–2448.
- (10) Wang, H.; Oehlschlaeger, M. A. Autoignition Studies of Conventional and Fischer–Tropsch Jet Fuels. *Fuel* **2012**, *98*, 249–258.
- (11) Merrill, E. A.; Gearhart, J. M.; Sterner, T. R.; Robinson, P. J. Improved Predictive Model for *n*-Decane Kinetics across Species, as a Component of Hydrocarbon Mixtures. *Inhalation Toxicol.* **2008**, *20*, 851–863.
- (12) Holley, A. T.; Dong, Y.; Andac, M. G.; Egolfopoulos, F. N.; Edwards, T. Ignition and Extinction of Non-Premixed Flames of Single-Component Liquid Hydrocarbons, Jet Fuels, and Their Surrogates. *Proc. Combust. Inst.* **2007**, *31*, 1205–1213.
- (13) Pitz, W. J.; Cernansky, N. P.; Dryer, F. L.; Egolfopoulos, F. N.; Farrell, J. T.; Friend, D. G.; Pitsch, H., *Development of an Experimental Database and Chemical Kinetic Models for Surrogate Gasoline Fuels*; SAE International: 2007.
- (14) Allen, C.; Valco, D.; Toulson, E.; Edwards, T.; Lee, T. Ignition Behavior and Surrogate Modeling of JP-8 and of Camelina and Tallow Hydrotreated Renewable Jet Fuels at Low Temperatures. *Combust. Flame* **2013**, *160*, 232–239.
- (15) Natelson, R. H.; Kurman, M. S.; Johnson, R. O.; Cernansky, N. P.; Miller, D. L. Preignition and Autoignition Chemistry of the Xylene Isomers. *Combust. Sci. Technol.* **2011**, *183*, 897–914.
- (16) Joklik, R.; Fuller, C.; Turner, B.; Gokulakrishnan, P. In *The Effect of Multi-Component Fuel Evaporation on the Ignition of JP-8. Proceedings of the ASME Turbo Expo: Power for Land, Sea, and Air*; ASME: 2010.
- (17) Honnet, S.; Seshadri, K.; Niemann, U.; Peters, N. A Surrogate Fuel for Kerosene. *Proc. Combust. Inst.* **2009**, *32*, 485–492.
- (18) Tosatto, L.; Mantia, B. L.; Bufferand, H.; Duchaine, P.; Gomez, A. Chemical Structure of a Methane Counterflow Diffusion Flame Perturbed with the Addition of either JP-8 or a Jet Fuel Surrogate. *Proc. Combust. Inst.* **2009**, *32*, 1319–1326.
- (19) Lenhart, D. B.; Miller, D. L.; Cernansky, N. P. The Oxidation of JP-8, Jet-A, and Their Surrogates in the Low and Intermediate Temperature Regime at Elevated Pressures. *Combust. Sci. Technol.* **2007**, *179*, 845–861.
- (20) Kahandawala, M. S. P.; DeWitt, M. J.; Corporan, E.; Sidhu, S. S. Ignition and Emission Characteristics of Surrogate and Practical Jet Fuels. *Energy Fuels* **2008**, *22*, 3673–3679.
- (21) Katta, V. R.; Roquemore, W. M. In Performance of JP-8 Surrogates and Parent Species in a Swirl Combustor. *Proceedings of the ASME Turbo Expo: Power for Land, Sea, and Air*; ASME: 2010.
- (22) Ji, C.; Sarathy, S. M.; Veloo, P. S.; Westbrook, C. K.; Egolfopoulos, F. N. Effects of Fuel Branching on the Propagation of Cctane Isomers Flames. *Combust. Flame* **2012**, *159*, 1426–1436.
- (23) Natelson, R. H.; Johnson, R. O.; Kurman, M. S.; Cernansky, N. P.; Miller, D. L. Comparison of Reactivity in a Flow Reactor and a Single Cylinder Engine. *Exp. Therm. Fluid Sci.* **2010**, *34*, 928–932.
- (24) Mensch, A.; Santoro, R. J.; Litzinger, T. A.; Lee, S. Y. Sooting Characteristics of Surrogates for Jet Fuels. *Combust. Flame* **2010**, *157*, 1097–1105.
- (25) Tremblay, R. T.; Martin, S. A.; Fisher, J. W. Novel Characterization of the Aerosol and Gas-Phase Composition of Aerosolized Jet Fuel. *Inhalation Toxicol.* **2010**, *22*, 394–401.
- (26) Mawid, M. A.; Park, T. W.; Sekar, B.; Arana, C. In *Development and Validation of a Detailed JP-8 Fuel Chemistry Model*. Presented at the 2nd JANNAF Modeling and Simulation Subcommittee Meeting, Destin, FL.
- (27) Tosatto, L.; Mella, F.; Long, M. B.; Smooke, M. D. A Study of JP-8 Surrogate Coflow Flame Structure by Combined Use of Laser Diagnostics and Numerical Simulation. *Combust. Flame* **2012**, *159*, 3027–3039.
- (28) Miller, J. A.; Pilling, M. J.; Troe, J. Unravelling Combustion Mechanisms Through a Quantitative Understanding of Elementary Reactions. *Proc. Combust. Inst.* **2005**, *30*, 43–88.
- (29) Violi, A.; Yan, S.; Eddings, E. G.; Sarofim, F.; Granata, S.; Faravelli, T.; Ranzi, E. Experimental Formulation and Kinetic Model for JP-8 Surrogate Mixtures. *Combust. Sci. Technol.* **2002**, *174*, 399–417.
- (30) Podlesak, T.; Hendrickson, M.; Matthews, S.; Nawrocki, E.; Seibert, M.; Zalewski, M. Army Stirling Engine Research and Development - Past, Present and Future. *Power Sources Conference* **2010**, *44*, 462–465.
- (31) Singh, D.; Nishiie, T.; Qiao, L. Experimental and Kinetic Modeling Study of the Combustion of *n*-Decane, Jet-A, and S-8 in Laminar Premixed Flames. *Combust. Sci. Technol.* **2011**, *183*, 1002–1026.
- (32) Liu, N.; Ji, C.; Egolfopoulos, F. N. Ignition of Non-Premixed C3–C12 *n*-Alkane Flames. *Combust. Flame* **2012**, *159*, 465–475.
- (33) Ji, C.; Dames, E.; Wang, Y. L.; Wang, H.; Egolfopoulos, F. N. Propagation and Extinction of Premixed C5–C12 *n*-Alkane Flames. *Combust. Flame* **2010**, *157*, 277–287.
- (34) Pilla, G. L.; Davidson, D. F.; Hanson, R. K. Shock Tube/Laser Absorption Measurements of Ethylene Time-Histories during Ethylene and *n*-Heptane Pyrolysis. *Proc. Combust. Inst.* **2011**, *33*, 333–340.
- (35) Sarathy, S. M.; Westbrook, C. K.; Mehl, M.; Pitz, W. J.; Togbe, C.; Dagaut, P.; Wang, H.; Oehlschlaeger, M. A.; Niemann, U.; Seshadri, K.; et al. Comprehensive Chemical Kinetic Modeling of the Oxidation of 2-Methylalkanes from C7 to C20. *Combust. Flame* **2011**, *158*, 2338–2357.
- (36) Holley, A. T.; You, X. Q.; Dames, E.; Wang, H.; Egolfopoulos, F. N. Sensitivity of Propagation and Extinction of Large Hydrocarbon Flames to Fuel Diffusion. *Proc. Combust. Inst.* **2009**, *32*, 1157–1163.
- (37) You, X.; Egolfopoulos, F. N.; Wang, H. Detailed and Simplified Kinetic Models of *n*-Dodecane Oxidation: The Role of Fuel Cracking in Aliphatic Hydrocarbon Combustion. *Proc. Combust. Inst.* **2009**, *32*, 403–410.
- (38) Malewicki, T.; Brezinsky, K. Experimental and Modeling Study on the Pyrolysis and Oxidation of *n*-Decane and *n*-Dodecane. *Proc. Combust. Inst.* **2013**, *34*, 361–368.

- (39) Zeng, M.; Yuan, W.; Wang, Y.; Zhou, W.; Zhang, L.; Qi, F.; Li, Y. Experimental and Kinetic Modeling Study of Pyrolysis and Oxidation of *n*-Decane. *Combust. Flame* **2014**, *161*, 1701–1715.
- (40) Cool, T. A.; McIlroy, A.; Qi, F.; Westmoreland, P. R.; Poisson, L.; Peterka, D. S.; Ahmed, M. Photoionization Mass Spectrometer for Studies of Flame Chemistry With a Synchrotron Light Source. *Rev. Sci. Instrum.* **2005**, *76*, 094102.
- (41) Qi, F.; Yang, R.; Yang, B.; Huang, C. Q.; Wei, L. X.; Wang, J.; Sheng, L. S.; Zhang, Y. W. Isomeric Identification of Polycyclic Aromatic Hydrocarbons Formed in Combustion With Tunable Vacuum Ultraviolet Photoionization. *Rev. Sci. Instrum.* **2006**, *77*, 084101.
- (42) Yang, B.; Li, Y. Y.; Wei, L. X.; Huang, C. Q.; Wang, J.; Tian, Z. Y.; Yang, R.; Sheng, L. S.; Zhang, Y. W.; Qi, F. An Experimental Study of The Premixed Benzene/Oxygen/Argon Flame With Tunable Synchrotron Photoionization. *Proc. Combust. Inst.* **2007**, *31*, 555–563.
- (43) Yang, B.; Oßwald, P.; Li, Y.; Wang, J.; Wei, L.; Tian, Z.; Qi, F.; Kohse-Höinghaus, K. Identification of Combustion Intermediates in Isomeric Fuel-Rich Premixed Butanol–Oxygen Flames at Low Pressure. *Combust. Flame* **2007**, *148*, 198–209.
- (44) Li, Y. Y.; Zhang, L. D.; Tian, Z. Y.; Yuan, T.; Wang, J.; Yang, B.; Qi, F. Experimental Study of a Fuel-Rich Premixed Toluene Flame at Low Pressure. *Energy Fuels* **2009**, *23*, 1473–1485.
- (45) Li, Y. Y.; Zhang, L. D.; Tian, Z. Y.; Yuan, T.; Zhang, K. W.; Yang, B.; Qi, F. Investigation of The Rich Premixed Laminar Acetylene/Oxygen/Argon Flame: Comprehensive Flame Structure and Special Concerns of Polyynes. *Proc. Combust. Inst.* **2009**, *32*, 1293–1300.
- (46) Li, Y. Y.; Qi, F. Recent Applications of Synchrotron VUV Photoionization Mass Spectrometry: Insight into Combustion Chemistry. *Acc. Chem. Res.* **2010**, *43*, 68–78.
- (47) Zhang, L. D.; Cai, J. H.; Zhang, T. C.; Qi, F. Kinetic Modeling Study of Toluene Pyrolysis at Low Pressure. *Combust. Flame* **2010**, *157*, 1686–1697.
- (48) Qi, F. Combustion Chemistry Probed by Synchrotron VUV Photoionization Mass Spectrometry. *Proc. Combust. Inst.* **2013**, *34*, 33–63.
- (49) Zeppieri, S. P.; Klotz, S. D.; Dryer, F. L. Modeling Concepts for Larger Carbon Number Alkanes: A Partially Reduced Skeletal Mechanism for *n*-Decane Oxidation and Pyrolysis. *Proc. Combust. Inst.* **2000**, *28*, 1587–1595.
- (50) Jia, Z. J.; Huang, H. Y.; Zhou, W. X.; Qi, F.; Zeng, M. R. Experimental and Modeling Investigation of *n*-Decane Pyrolysis at Supercritical Pressures. *Energy Fuels* **2014**, *28*, 6019–6028.
- (51) Jia, Z.; Wang, Z.; Cheng, Z.; Zhou, W. Experimental and Modeling Study on Pyrolysis of *n*-Decane Initiated by Nitromethane. *Combust. Flame* **2016**, *165*, 246–258.
- (52) Zhu, Y. H.; Liu, B.; Jiang, P. X. Experimental and Numerical Investigations on *n*-Decane Thermal Cracking at Supercritical Pressures in a Vertical Tube. *Energy Fuels* **2014**, *28*, 466–474.
- (53) Rumyantsev, A. N.; Shevel'kova, L. V.; Sokolova, V. M.; Nametkin, N. S. Dependence of the Decomposition Rate Constant of Higher *n*-Paraffin Hydrocarbons on Their Molecular Weight. *Neftekhimiya* **1980**, *20*, 212–217.
- (54) Gloria, G. M.; Lew, L.; Cunningham, R. E. Determinación De La Cinética De Descomposición Térmica De Alcoholes E Hidrocarburos Mediante Un Reactor Pulso. *Lab. Ensayo Mater. Invest. Tecnol. Prov. Buenos Aires Publ. Ser.* **1971**, *2*, 103–123.
- (55) Zhou, Z. Y.; Zhang, L. D.; Xie, M. F.; Wang, Z. D.; Chen, D. N.; Qi, F. Determination of Absolute Photoionization Cross-Sections of Alkanes and Cyclo-Alkanes. *Rapid Commun. Mass Spectrom.* **2010**, *24*, 1335–1342.
- (56) Wang, F.; Ren, J.; Li, Y. W. Enthalpies of Formation and C-C Bond Dissociation Energies of C1-C14 Alkanes and Alkyl Radicals Calculated Via Density Functional Theory Methods. *Chin. J. Appl. Chem.* **2009**, *26*, 1484–1488.
- (57) Song, J. W.; Tsuneda, T.; Sato, T.; Hirao, K. Calculations of Alkane Energies Using Long-Range Corrected DFT Combined with Intramolecular van der Waals Correlation. *Org. Lett.* **2010**, *12*, 1440–1443.
- (58) Ranzi, E.; Frassoldati, A.; Granata, S.; Faravelli, T. Wide-Range Kinetic Modeling Study of the Pyrolysis, Partial Oxidation, and Combustion of Heavy *n*-Alkanes. *Ind. Eng. Chem. Res.* **2005**, *44*, 5170–5183.
- (59) Ranzi, E.; Faravelli, T.; Gaffuri, P.; Garavaglia, E.; Goldaniga, A. Primary Pyrolysis and Oxidation Reactions of Linear and Branched Alkanes. *Ind. Eng. Chem. Res.* **1997**, *36*, 3336–3344.
- (60) Westbrook, C. K.; Pitz, W. J.; Herbinet, O.; Curran, H. J.; Silke, E. J. A Comprehensive Detailed Chemical Kinetic Reaction Mechanism for Combustion of *n*-Alkane Hydrocarbons from *n*-Octane to *n*-Hexadecane. *Combust. Flame* **2009**, *156*, 181–199.
- (61) Dooley, S.; Won, S. H.; Chaos, M.; Heyne, J.; Ju, Y. G.; Dryer, F. L.; Kumar, K.; Sung, C. J.; Wang, H. W.; Oehlschlaeger, M. A.; et al. A Jet Fuel Surrogate Formulated by Real Fuel Properties. *Combust. Flame* **2010**, *157*, 2333–2339.
- (62) Russo, M. F.; van Duin, A. C. T. Molecular Dynamics Simulations of Aromatic Hydrocarbon Combustion via the ReaxFF Reactive Force Field. *Abstr. Pap. (Am. Chem. Soc.)* **2010**, *240*, 1.
- (63) Zhang, F. T.; Kaiser, R. I.; Kislov, V. V.; Mebel, A. M.; Golan, A.; Ahmed, M. A VUV Photoionization Study of the Formation of the Indene Molecule and Its Isomers. *J. Phys. Chem. Lett.* **2011**, *2*, 1731–1735.
- (64) Zhang, F. T.; Kaiser, R. I.; Golan, A.; Ahmed, M.; Hansen, N. A VUV Photoionization Study of the Combustion-Relevant Reaction of the Phenyl Radical (C<sub>6</sub>H<sub>5</sub>) with Propylene (C<sub>3</sub>H<sub>6</sub>) in a High Temperature Chemical Reactor. *J. Phys. Chem. A* **2012**, *116*, 3541–3546.
- (65) Kaiser, R. I.; Belau, L.; Leone, S. R.; Ahmed, M.; Wang, Y. M.; Braams, B. J.; Bowman, J. M. A Combined Experimental and Computational Study on the Ionization Energies of the Cyclic and Linear C<sub>3</sub>H Isomers. *ChemPhysChem* **2007**, *8*, 1236–1239.
- (66) Kaiser, R. I.; Mebel, A.; Kostko, O.; Ahmed, M. On the Ionization Energies of C<sub>4</sub>H<sub>3</sub> Isomers. *Chem. Phys. Lett.* **2010**, *485*, 281–285.
- (67) Kaiser, R. I.; Sun, B. J.; Lin, H. M.; Chang, A. H. H.; Mebel, A. M.; Kostko, O.; Ahmed, M. An Experimental and Theoretical Study of the Ionization Energies of Polyynes (H-(C≡C)<sub>n</sub>-H; n= 1–9). *Astrophys. J.* **2010**, *719*, 1884–1889.
- (68) Kaiser, R. I.; Maksyutenko, P.; Ennis, C.; Zhang, F. T.; Gu, X. B.; Krishtal, S. P.; Mebel, A. M.; Kostko, O.; Ahmed, M. Untangling the Chemical Evolution of Titan's Atmosphere and Surface-from Homogeneous to Heterogeneous Chemistry. *Faraday Discuss.* **2010**, *147*, 429–478.
- (69) Kaiser, R. I.; Krishtal, S. P.; Mebel, A. M.; Kostko, O.; Ahmed, M. An Experimental and Theoretical Study of the Ionization Energies of SiC<sub>2</sub>H<sub>x</sub> (x= 0, 1, 2) Isomers. *Astrophys. J.* **2012**, *761*, 178–184.
- (70) Golan, A.; Ahmed, M.; Mebel, A. M.; Kaiser, R. I. A VUV Photoionization Study of the Multichannel Reaction of Phenyl Radicals with 1,3-Butadiene under Combustion Relevant Conditions. *Phys. Chem. Chem. Phys.* **2013**, *15*, 341–347.
- (71) Kostko, O.; Zhou, J.; Sun, B. J.; Lie, J. S.; Chang, A. H. H.; Kaiser, R. I.; Ahmed, M. Determination of Ionization Energies of C<sub>n</sub>N (n= 4–12): Vacuum Ultraviolet Photoionization Experiments and Theoretical Calculations. *Astrophys. J.* **2010**, *717*, 674–682.
- (72) Parker, D. S.; Kaiser, R. I.; Troy, T. P.; Ahmed, M. Hydrogen Abstraction/Acetylene Addition Revealed. *Angew. Chem., Int. Ed.* **2014**, *53*, 7740–7744.
- (73) Urness, K. N.; Guan, Q.; Golan, A.; Daily, J. W.; Nimlos, M. R.; Stanton, J. F.; Ahmed, M.; Ellison, G. B. Pyrolysis of Furan in a Microreactor. *J. Chem. Phys.* **2013**, *139*, 124305.
- (74) Guan, Q.; Urness, K. N.; Ormond, T. K.; David, D. E.; Ellison, G. B.; Daily, J. W. The Properties of a Micro-Reactor for the Study of the Unimolecular Decomposition of Large Molecules. *Int. Rev. Phys. Chem.* **2014**, *33*, 447–487.
- (75) Cool, T. A.; Nakajima, K.; Taatjes, C. A.; McIlroy, A.; Westmoreland, P. R.; Law, M. E.; Morel, A. Studies of a Fuel-Rich

Propane Flame With Photoionization Mass Spectrometry. *Proc. Combust. Inst.* **2005**, *30*, 1681–1688.

(76) Cool, T. A.; Wang, J.; Nakajima, K.; Taatjes, C. A.; McLroy, A. Photoionization Cross Sections for Reaction Intermediates in Hydrocarbon Combustion. *Int. J. Mass Spectrom.* **2005**, *247*, 18–27.

(77) Oßwald, P.; Güldenbergh, H.; Kohse-Höinghaus, K.; Yang, B.; Yuan, T.; Qi, F. Combustion of Butanol Isomers – A Detailed Molecular Beam Mass Spectrometry Investigation of Their Flame Chemistry. *Combust. Flame* **2011**, *158*, 2–15.

(78) Photoionization Cross Section Database (Version 1.0). National Synchrotron Radiation Laboratory: Hefei, China. <http://flame.nslr.ustc.edu.cn/database/>; 2011.

(79) Curtiss, L. A.; Raghavachari, K.; Redfern, P. C.; Rassolov, V.; Pople, J. A. Gaussian-3 (G3) Theory for Molecules Containing First and Second-Row Atoms. *J. Chem. Phys.* **1998**, *109*, 7764–7776.

(80) Baboul, A. G.; Curtiss, L. A.; Redfern, P. C.; Raghavachari, K. Gaussian-3 Theory Using Density Functional Geometries and Zero-Point Energies. *J. Chem. Phys.* **1999**, *110*, 7650–7657.

(81) Curtiss, L. A.; Raghavachari, K.; Redfern, P. C.; Baboul, A. G.; Pople, J. A. Gaussian-3 Theory Using Coupled Cluster Energies. *Chem. Phys. Lett.* **1999**, *314*, 101–107.

(82) Frisch, M. J.; Trucks, G. W.; Schlegel, H. B.; Scuseria, G. E.; Robb, M. A.; Cheeseman, J. R.; Scalmani, G.; Barone, V.; Mennucci, B.; Petersson, G. A.; et al. *Gaussian 09, Revision A.1*; Gaussian Inc.: Wallingford CT, 2009.

(83) Werner, H. J.; Knowles, P. J.; Knizia, G.; Manby, F. R.; Schütz, M.; Celani, P.; Gyröffy, W.; Kats, D.; Korona, T.; Lindh, R.; et al. *MOLPRO*, version 2010.1, a package of ab initio programs; <http://www.molpro.net>.

(84) Georgievskii, Y.; Miller, J. A.; Burke, M. P.; Klippenstein, S. J. Reformulation and Solution of the Master Equation for Multiple-Well Chemical Reactions. *J. Phys. Chem. A* **2013**, *117*, 12146–12154.

(85) Georgievskii, Y.; Klippenstein, S. J. MESS.2016.3.23, <http://tcg.cse.anl.gov/papr/codes/mess.html>.

(86) Troe, J. Theory of Thermal Unimolecular Reactions at Low Pressures. I. Solutions of the Master Equation. *J. Chem. Phys.* **1977**, *66*, 4745–4757.

(87) Jasper, A. W.; Oana, C. M.; Miller, J. A. Third-Body” Collision Efficiencies for Combustion Modeling: Hydrocarbons in Atomic and Aiatomic Baths. *Proc. Combust. Inst.* **2015**, *35*, 197–204.

(88) Jasper, A. W.; Miller, J. A. Lennard–Jones Parameters for Combustion and Chemical Kinetics Modeling from Full-Dimensional Intermolecular Potentials. *Combust. Flame* **2014**, *161*, 101–110.

(89) Klippenstein, S. J.; Georgievskii, Y.; Harding, L. B. Predictive Theory for the Combination Kinetics of Two Alkyl Radicals. *Phys. Chem. Chem. Phys.* **2006**, *8*, 1133–1147.

(90) Harding, L. B.; Georgievskii, Y.; Klippenstein, S. J. Predictive Theory for Hydrogen Atom - Hydrocarbon Radical Association Kinetics. *J. Phys. Chem. A* **2005**, *109*, 4646–4656.

(91) Active Thermochemical Tables: <http://atct.anl.gov/Thermochemical%20Data/version%201.118/index.php>.

(92) Tsang, W.; Walker, J. A.; Manion, J. A. The Decomposition of Normal Hexyl Radicals. *Proc. Combust. Inst.* **2007**, *31*, 141–148.

(93) Tsang, W.; McGovern, W. S.; Manion, J. A. Multichannel Decomposition and Isomerization of Octyl Radicals. *Proc. Combust. Inst.* **2009**, *32*, 131–138.

(94) Sivaramakrishnan, R.; Michael, J. V.; Ruscic, B. High-Temperature Rate Constants for H/D + C<sub>2</sub>H<sub>6</sub> and C<sub>3</sub>H<sub>8</sub>. *Int. J. Chem. Kinet.* **2012**, *44*, 194–205.

(95) Tsang, W. Chemical Kinetic Data-Base for Combustion Chemistry. Part 3. Propane. *J. Phys. Chem. Ref. Data* **1988**, *17*, 887–952.

(96) Baldwin, R. R.; Walker, R. W. Rate Constants for Hydrogen + Oxygen System, and for H Atoms and OH Radicals + Alkanes. *J. Chem. Soc., Faraday Trans. 1* **1979**, *75*, 140–154.

(97) Stewart, J.; Brezinsky, K.; Glassman, I. Supercritical Pyrolysis of Decalin, Tetralin, and *n*-Decane at 700–800K. Product Distribution and Reaction Mechanism. *Combust. Sci. Technol.* **1998**, *136*, 373–390.

(98) Glassman, I.; Yetter, R. A.; Glumac, N. G. *Combustion*; Academic Press: 2014.

(99) Chang, A. H. H.; Mebel, A. M.; Yang, X. M.; Lin, S. H.; Lee, Y. T. Ab Initio/RRKM Approach Toward the Understanding of Ethylene Photodissociation. *J. Chem. Phys.* **1998**, *109*, 2748–2761.

(100) Narendrapurapu, B. S.; Simmonett, A. C.; Schaefer, H. F., III; Miller, J. A.; Klippenstein, S. J. Combustion Chemistry: Important Features of the C<sub>3</sub>H<sub>5</sub> Potential Energy Surface, Including Allyl Radical, Propargyl + H<sub>2</sub>, Allene + H, and Eight Transition States. *J. Phys. Chem. A* **2011**, *115*, 14209–14214.

(101) Hansen, N.; Miller, J. A.; Westmoreland, P. R.; Kasper, T.; Kohse-Hoinghaus, K.; Wang, J.; Cool, T. A. Isomer-Specific Combustion Chemistry in Allene and Propyne Flames. *Combust. Flame* **2009**, *156*, 2153–2164.

(102) Miller, J. A.; Senosiain, J. P.; Klippenstein, S. J.; Georgievskii, Y. Reactions over Multiple, Interconnected Potential Wells: Unimolecular and Bimolecular Reactions on a C<sub>3</sub>H<sub>5</sub> Potential. *J. Phys. Chem. A* **2008**, *112*, 9429–9438.

(103) Chin, C. H.; Lee, S. H. Comparison of Two-Body and Three-Body Decomposition of Ethanedial, Propanal, Propenal, *n*-Butane, 1-Butene, and 1,3-Butadiene. *J. Chem. Phys.* **2012**, *136*, 024308.

(104) Ribeiro, J. M.; Mebel, A. M. Reaction Mechanism and Product Branching Ratios of the CH + C<sub>3</sub>H<sub>6</sub> Reaction: A Theoretical Study. *J. Phys. Chem. A* **2016**, *120*, 1800–1812.

(105) Backx, C.; Wight, G. R.; Wiel, M. J. V. d. Oscillator Strengths (10–70 eV) for Absorption, Ionization and Dissociation in H<sub>2</sub>, HD and D<sub>2</sub>, Obtained by an Electron-Ion Coincidence Method. *J. Phys. B: At. Mol. Phys.* **1976**, *9*, 315.

(106) Savee, J. D.; Soorkia, S.; Welz, O.; Selby, T. M.; Taatjes, C. A.; Osborn, D. L. Absolute Photoionization Cross-Section of the Propargyl Radical. *J. Chem. Phys.* **2012**, *136*, 134307.

(107) Samson, J. A. R.; Haddad, G. N.; Masuoka, T.; Pareek, P. N.; Kilcoyne, D. A. L. Ionization Yields, Total Absorption, and Dissociative Photoionization Cross-Sections of CH<sub>4</sub> from 110–950-Å. *J. Chem. Phys.* **1989**, *90*, 6925–6932.

(108) Robinson, J. C.; Sveum, N. E.; Neumark, D. M. Determination of Absolute Photoionization Cross Sections for Vinyl and Propargyl Radicals. *J. Chem. Phys.* **2003**, *119*, 5311–5314.

(109) Gans, B.; Garcia, G. A.; Boyé-Péronne, S.; Loison, J.-C.; Douin, S.; Gaie-Levrel, F.; Gauyacq, D. Absolute Photoionization Cross Section of the Ethyl Radical in the Range 8–11.5 eV: Synchrotron and Vacuum Ultraviolet Laser Measurements. *J. Phys. Chem. A* **2011**, *115*, 5387–5396.

(110) Yang, B.; Wang, J.; Cool, T. A.; Hansen, N.; Skeen, S.; Osborn, D. L. Absolute Photoionization Cross-Sections of Some Combustion Intermediates. *Int. J. Mass Spectrom.* **2012**, *309*, 118–128.

(111) Robinson, J. C.; Sveum, N. E.; Neumark, D. M. Determination of Absolute Photoionization Cross Sections for Isomers of C<sub>3</sub>H<sub>5</sub>: Allyl and 2-Propenyl Radicals. *Chem. Phys. Lett.* **2004**, *383*, 601–605.

(112) Koizumi, H. Predominant Decay Channel for Superexcited Organic-Molecules. *J. Chem. Phys.* **1991**, *95*, 5846–5852.

(113) Wang, J.; Yang, B.; Cool, T. A.; Hansen, N.; Kasper, T. Near-Threshold Absolute Photoionization Cross-Sections of Some Reaction Intermediates in Combustion. *Int. J. Mass Spectrom.* **2008**, *269*, 210–220.